PRECIPITATION PHASE PARTITIONING WITH A PSYCHROMETRIC ENERGY BALANCE:

MODEL DEVELOPMENT AND APPLICATION

A Thesis Submitted to the

College of Graduate Studies and Research

in Partial Fulfillment of the Requirements

for the Degree of Master of Science

in the Department of Geography and Planning

(Centre for Hydrology)

University of Saskatchewan, Saskatoon

By Phillip Harder

Permission to Use

In presenting this thesis in partial fulfilment of the requirements for a Postgraduate degree from the University of Saskatchewan, I agree that the Libraries of this University may make it freely available for inspection. I further agree that permission for copying of this thesis in any manner, in whole or in part, for scholarly purposes may be granted by the professor or professors who supervised my thesis work or, in their absence, by the Head of the Department or the Dean of the College in which my thesis work was done. It is understood that any copying or publication or use of this thesis or parts thereof for financial gain shall not be allowed without my written permission. It is also understood that due recognition shall be given to me and to the University of Saskatchewan in any scholarly use which may be made of any material in my thesis.

Requests for permission to copy or to make other use of material in this thesis in whole or part should be addressed to:

Head of the Department of Geography and Planning
117 Science Place
University of Saskatchewan
Saskatoon, SK Canada
S7N 5C8

Abstract

Precipitation phase is fundamental to a catchment's hydrological response to precipitation events in cold regions and is especially variable over time and space in complex topography. Phase is controlled by the microphysics of the falling hydrometeor, but microphysical calculations require detailed atmospheric information that is often unavailable and lacking from hydrological analyses. In hydrology, there have been many methods developed to estimate phase, but most are regionally calibrated and many depend on air temperature (T_a) and use daily time steps. Phase is not only related to T_a, but to other meteorological variables such as humidity. In addition, precipitation events are dynamic, adding uncertainties to the use of daily indices to estimate phase. To better predict precipitation phase with respect to meteorological conditions, the combined mass and energy balance of a falling hydrometeor was calculated and used to develop a model to estimate precipitation phase. Precipitation phase and meteorological data were observed at multiple elevations in a small Canadian Rockies catchment, Marmot Creek Research Basin, at 15-minute intervals over several years to develop and test the model. The mass and energy balance model was compared to other methods over varying time scales, seasons, elevations and topographic exposures. The results indicate that the psychrometric energy balance model performs much better than T_a methods and that this improvement increases as the calculation time interval decreases. The uncertainty that differing phase methods introduce to hydrological process estimation was assessed with the Cold Regions Hydrological Model (CRHM). The rainfall/total precipitation ratio, runoff, discharge and snowpack accumulation were calculated using a single and a double T_a threshold method and the proposed physically based mass and energy balance model. Intercomparison of the hydrological responses of the methods highlighted differences between T_a based and psychrometric approaches. Uncertainty of hydrological processes, as established by simulating a wide range of T_a methods, reached up to 20% for rain ratio, 1.5 mm for mean daily runoff, 0.4 mm for mean daily discharge and 160 mm of peak snow water equivalent. The range of T_a methods showed that snowcover duration, snow free date and peak discharge date could vary by up to 36, 26 and 10 days respectively. The greatest hydrological uncertainty due to precipitation phase methods was found at sub-alpine and sub-arctic headwater basins and the least uncertainty was found at a small prairie basin.

Acknowledgements

This project would not have been possible without the contributions of many individuals and organizations. First and foremost, the data collection at Marmot Creek Research Basin since 2005, coordinated by the Centre for Hydrology field technicians Mike Solohub and May Guan, was invaluable. The many students who spent countless hours in the field contributing to the data collection program are also gratefully acknowledged.

I wish to thank my fellow grad students, namely Evan Siemens and Dhiraj Pradhananga for the camaraderie and in making the coursework and trips enjoyable and Chris Marsh for his valuable feedback and in-depth conversations.

I would like to thank my committee members, Dr. Kevin Shook for his insights on R and all things hydrology and Dr. Warren Helgason, for his valuable commentary throughout this project. I would like to acknowledge my supervisor, Dr. John Pomeroy, for his encouragement in my pursuing graduate studies, his enthusiasm in hydrology and for his high standards which makes for an excellent research program of which I am honored to be a part.

Funding to make this project possible came from the University of Saskatchewan and the National Science and Engineering Research Council through a post graduate scholarship and the Canada Research Chairs program. I am also grateful to the community of contributors to R, an open source statistical program, which was used to conduct all of the analysis in this thesis.

Lastly I wish to acknowledge the patient and motivating support of my wife Kristen Harder. The many hours of proof reading and the support during the busy times inspires me to do the best work that I can.

To Kristen and Everett.

Table of Contents

List of Tables

List of Figures

List of Abbreviations

BGSI	Biogeoscience Institute Barrier Lake Field Station
BL	Bad Lake
CRHM	Cold Regions Hydrological Modeling platform
FR	Fisera Ridge
FO	Fisera Ridge Forest
GB	Granger Basin
HSPF	USGS Hydrological Simulation Program Fortran method
HM	Hay Meadow
HRU	Hydrological Response Unit
KS	Kolmogorov-Smirnov
MB	Mean Bias
MC	Marmot Creek Research Basin
PSY	Proposed Psychrometric Phase Parameterisation
RMSD	Root Mean Square Difference
RT	Fisera Ridge Ridgetop
SWE	Snow Water Equivalent
TBRG	Tipping Bucket Rain Gauge
T0	Single Air Temperature Threshold Method
Ti0	Single Hydrometeor Temperature Threshold Method
UBC	Pipes and Quick Double Threshold Temperature Method
UC	Upper Clearing
UF	Upper Forest
WC	Wolf Creek Research Basin

List of Symbols

c_p	Specific heat capacity of air [1.0035 kJ kg^{-1} K^{-1}]
D	Diffusivity of water vapour in air [m^2 s^{-1}]
dm	Change in hydrometeor mass [kg]
dt	Change in time [s]
e	Vapour pressure, actual (e_a) and saturated with respect to water (e_{satw}) and ice (e_{sati})[kPa]
f_r	Rainfall ratio [dimensionless]
i	Array index
L	Latent heat of sublimation (L_s) or vaporisation (L_v) [J kg^{-1}]
m_w	Molecular weight of water [0.01801528 kg mol^{-1}]
n	Number of values
Nu	Nusselt number [dimensionless]
p	Atmospheric pressure [kPa]
r	Hydrometeor radius [m]
R	Resistance to vapour (R_V) and heat (R_H) transfer
$\bar{R}$	Universal gas constant [8.31441 J mol^{-1} K^{-1}]
RH	Relative humidity [%]
Sh	Sherwood number [dimensionless]
T_a	Air temperature [°C or K]
T_d	Dewpoint temperature [°C or F]
T_i	Hydrometeor temperature [°C]
T_r	Transition temperature range [°C]
T_{ri}	Initial transition temperature range [°C]
T_s	Surface temperature of hydrometeor [K]
T_t	Rainfall-Snowfall threshold temperature [°C]
T_{ti}	Initial temperature threshold [°C or F]
T_w	Thermodynamic wet bulb temperature [°C]
X_o	Observed value
X_s	Simulated value

ρ	Water vapour density in the free atmosphere (ρ_{Ta}) and saturated at the hydrometeor surface($\rho_{sat(Ts)}$)[kg m^{-3}]
ε	Molecular ratio of water vapor to air [0.622]
γ	Psychrometric constant [~0.066 kPa K^{-1}]
γ^*	Modified psychrometric constant [kPa K^{-1}]
λ_t	Thermal conductivity of air [J m^{-1} s^{-1} K^{-1}]

CHAPTER 1. Introduction

1.1 Statement of Problem

Information pertaining to precipitation intensity, duration, quantity and phase is crucial to hydrological analysis and prediction in cold regions (Gray, 1970). The uncertainty of hydrological predictions is strongly influenced by the quality of the input data (Zehe *et al.,* 2005). Rainfall and snowfall initiate very different hydrologic processes which leads to large variations in catchment responses to precipitation events. Rainfall immediately begins to be separated by hydrological processes into evaporation, runoff and infiltration, ultimately leading to stream flow generation and to groundwater storage. In contrast, the hydrological response of a basin to snowfall is delayed by the seasonal snowpack accumulation and its subsequent melt. The rate of snowmelt input to other processes is moderated by the energy available for melt, but there is no moderation of a rainfall input. Rain on snow events require a detailed understanding of precipitation phase, as energy advection from rainfall to the snowpack can lead to large snowmelt rates which can significantly augment the runoff due to rainfall (Marks *et al.,* 1998). Precipitation phase varies widely over space and time and this heterogeneity is especially large in complex topography. Elevation exerts a strong control on air temperature (T_a) and consequently relative humidity (*RH*) which in turn controls precipitation phase. The elevation dependency of precipitation phase is best visualized in the snow line of a storm, the elevation where precipitation transitions from snow to rain, which is a consequence of the interaction of T_a and humidity lapse rates, meteorological mechanisms, upslope or downslope synoptic events and topography (Marks *et al.,* 2013; Minder *et al.,* 2011). Unfortunately, most automated meteorological stations do not directly observe precipitation phase but rather report rainfall or total precipitation. Identification of precipitation phase is required but there is no standardized approach to do this.

Commonly utilized methods to identify precipitation phase in hydrology rely on empirical correlation of surface T_a with observations of precipitation phase. Often these correlations are parameterised as thresholds which partition all precipitation as rainfall above, and as snowfall below, specific air temperatures. There are many problems with current empirical T_a

precipitation phase methods. Thresholds in T_a methods are based upon observation, or calibrations, at specific sites which limits their spatial transferability. When observations of phase are not available, T_a thresholds are often assigned arbitrarily. Phase partitioning approaches that are restricted to T_a ignore important physical processes controlling precipitation phase by not incorporating observations of humidity. All precipitation phase methods restricted to near surface observations are simplistic and do not fully represent precipitation phase processes as precipitation phase is controlled by atmospheric processes. The uncertainties introduced by these precipitation phase partitioning methods are unknown and need to be quantified to improve hydrological modelling.

The 2013 flooding in Alberta demonstrates the effect of precipitation phase on hydrological responses. Over the interval of June 19-22 2013, portions of Southwestern Alberta received in excess of 300 mm of precipitation (AESRD, 2013) leading to catastrophic flooding which caused 100,000 people to be evacuated, 4 fatalities and damage estimated to be up to $5 billion (Livingstone, 2013). The majority of precipitation came as rainfall, which was augmented by snowmelt from rain on snow in the upper reaches of the basin, leading to rapid flooding. Transition from rainfall to snowfall at higher elevation with cooling T_a was observed at the end of the event which decreased runoff generation (J. Pomeroy, personal communication, June 21, 2013). Understanding when and where this transition to snowfall took place is useful from a hydrological and a flood management perspective. If the transition had occurred earlier in the event the streamflow generated would have been smaller in magnitude. From a flood forecasting perspective, had the operational forecast model estimated an earlier transition than had been observed, the subsequent forecast would have underestimated the streamflow, which could potentially have reduced the effectiveness of the downstream preparations.

1.2 Rationale

Although traditional methods to identify the phase of precipitation have been dependent on T_a methods, the fields of meteorology and micrometeorology have developed physical understandings of the controls on the phase of a hydrometeor, which is an individual ice or water particle. Examples of psychrometric phase partitioning approaches have been proposed in European and Asian hydrological literature (Steinacker, 1983; Sugaya, 1991). The rationale for

this thesis is to apply the known physics of hydrometeors to develop a more physically appropriate model, compared to empirical T_a models, to identify precipitation phase. A semi-physical model to identify precipitation phase is developed using hydrometeor mass and energy balances developed for snow sublimation modelling. The combined mass and energy balance takes into account the latent and sensible heat fluxes that act to modify the hydrometeor temperature which is physically related to the phase of the hydrometeor. The hydrometeor temperature is thereafter fitted to observations of phase. Utilizing the proposed model and selected empirical T_a methods, the identification of precipitation phase in a North American context and the uncertainty that is introduced into hydrological modeling is assessed.

1.3 Nature and Scope of Research

The phase of precipitation is a function of the atmospheric processes acting on a hydrometeor as it falls from the cloud to the surface. Recent scientific advances (Pietroniro *et al.,* 2007) allow the coupling of hydrological models and atmospheric models which can diagnose precipitation phase directly, but these approaches still have challenges in terms of scaling hydrological processes appropriately. A better phase partitioning method is needed as uncoupled hydrological models will always be required. As the observations typically available in uncoupled hydrological models are restricted to near the surface, this study will focus on the use of near surface observations to develop a phase partitioning model that can be readily implemented in uncoupled hydrological models. The phase partitioning model represents the well measured conditions in a mountain research basin in the Canadian Rockies. Analysis of modeling uncertainty will consider a selection of small headwater research basins located in western Canada.

1.4 Objectives

Given the use of surface observations to quantify an atmospheric process and the practical difficulties associated with applying empirical techniques to separate precipitation by phase, the objectives of this thesis are:

1. To propose a combined energy and mass balance model to estimate precipitation phase that is consistent with the known thermodynamics of falling hydrometeors.

2. To assess the accuracy and temporal scale dependence of this phase estimation model using field measurements and compare the model to various approaches used in hydrological practice.
3. To quantify the uncertainties that empirical phase methods introduce into cold regions hydrological modelling.

The overall goal of the thesis is to propose a semi-physical, spatially transferable phase partitioning method, which can be readily implemented by hydrologists as an alternative to non-physical T_a methods. To address the objectives, the remainder of the thesis is divided into four chapters. Chapter 2 comprises the literature review which addresses the physics of precipitation phase, commonly utilized phase methods in hydrological models and the sensitivity of hydrological processes to variations in phase methods. The physical relationship between precipitation phase and the hydrometeor temperature (T_i) is described with the derivation of the T_i from a psychrometric mass and energy balance approach. Chapter 3 describes the site characteristics, data quality assurance and control and methodology utilized to develop the proposed T_i phase model to address Objectives 1 and 2. Discussion focuses on the temporal scale dependence of precipitation phase and compares the proposed model to commonly implemented approaches. Chapter 4 addresses Objective 3 through a hydrological modeling exercise. Basin models, the modeling platform and the modeling approach are described and the relationships observed in the uncertainty analysis, model performance and the limitations of the modeling approach are discussed. Chapter 5 summarizes the findings of the previous sections and presents the conclusions of the thesis.

CHAPTER 2. Literature Review

2.1 Precipitation Phase Physics

The phase of precipitation at the ground surface is influenced by the properties of the atmosphere that precipitation must pass through. These properties include the temperature, vertical thickness of atmospheric layers, humidity, atmospheric stability, hydrometeor fall velocity, structure and size and interactions among hydrometeors (Gray and Prowse, 1992). The relative importance of these properties varies with synoptic conditions. The factors influencing phase in the condensation region of an air mass are of less influence to the phase at the surface than the characteristics of the rest of the atmosphere through which the hydrometeor travels (Thériault and Stewart, 2010). During its fall, a hydrometeor can be thought of as a drop of water (frozen or liquid) falling through a dynamic water vapour continuum. Latent heat is added to the hydrometeor through condensation or removed though evaporation or sublimation depending on the vapour pressure deficit and the ventilation of a falling hydrometeor, which is a function of its fall velocity and of the prevailing wind conditions within the atmosphere (Stewart, 1992). Sensible heat can also be added or removed primarily through forced convection which is driven by the temperature gradient between the hydrometeor and the atmosphere and which is enhanced by the ventilation of the hydrometeor falling through the atmosphere (Stewart, 1992). The sensible and latent heat fluxes determine the temperature and rate of mass and energy change of the hydrometeor which ultimately controls its phase. If the energy available is enough to supply the latent heat of fusion required to melt or freeze the hydrometeor, then the phase will change. Hydrometeors exist in a range of size distributions which can cause different precipitation types to exist concurrently and with differing rates of melt or refreezing, leading to mixed precipitation events (Thériault and Stewart, 2010). In temperate and cold region environments precipitation is typically formed in the atmosphere as a solid (snowfall) and the phase at the surface is determined by whether the snowfall melts into rainfall (liquid) or not (Stewart, 1992).

2.2 Precipitation Phase Methods

Several approaches have been developed to quantify the phase of precipitation. The most physically comprehensive approaches are typically implemented by numerical micro-physical schemes over multiple vertical layers in dynamic atmospheric models, such as numerical weather

models or general circulation models (Thériault and Stewart, 2010; Minder *et al.,* 2011). Conditions at the ground surface are often used to identify phase in hydrological models that are uncoupled from atmospheric processes (Feiccabrino and Lundberg, 2008). The full solutions implemented in atmospheric models to resolve the phase of hydrometeors require information on atmospheric conditions, topographic influences, atmospheric lapse rates and surface interactions with the atmosphere (Marks *et al.,* 2013), which has limited their application in hydrological models.

Precipitation phase partitioning methods specifically for hydrology have generally focused on relating the precipitation phase to mean values of meteorological variables measured near the ground surface. Early work by the US Army Corps of Engineers (1956) and Auer (1974) showed the snowfall to rainfall transition occurring for daily mean T_a varying between 0 °C and 6 °C. Many other approaches have been suggested since which vary in complexity. The simplest and most commonly used model is to define a single threshold that defines all precipitation as rainfall above, and snowfall below, a specified threshold T_a (Leavesley *et al.,* 1983). The method, hereafter referred to as T0, is:

$$T_a \geq T_t \mid Rainfall \tag{2.1}$$

$$T_a < T_t \mid Snowfall \tag{2.2}$$

T_t is the threshold air temperature which can range from -1 °C to 4 °C as a daily value (Saelthun, 1996). Values of T_t are site specific (Marks *et al.,* 2013) and dependent on atmospheric stability (Olafsson and Haraldsdottir, 2003) and the factors mentioned previously. Double thresholds are also used, where a lower threshold defines all precipitation as snowfall and an upper threshold defines all precipitation as rainfall with the range between thresholds considered to be mixed phase. Pipes and Quick (1977), in the UBC watershed model, suggest 0.6 °C and 3.6 °C as thresholds with a linear interpolation in the mixed phase range. The method, hereafter referred to as UBC, is:

$$T_a \geq 3.6 \mid Rainfall \tag{2.3}$$

$$0.6 > T_a < 3.6 \mid f_r = (T_a/3) - 0.2 \tag{2.4}$$

$$T_a \leq 0.6 \mid Snowfall \tag{2.5}$$

Where f_r is the rain ratio which is the ratio of rainfall divided by total precipitation (i.e. snowfall + rainfall). Kienzle (2008) proposed a more complex double threshold approach which uses a

seasonally variable curvilinear approach. The shape of the transition curve is parameterised by a T_t value (the T_a where rainfall and snowfall amounts are equal) and a transition temperature range (T_r) which quantifies the T_a range in which both rainfall and snowfall are observed. The method, hereafter referred to as Kienzle, is:

$$T_a \geq T_t \mid fr = 5 * \left(\frac{T - T_t}{1.4 * T_r}\right)^3 - 6.76 * \left(\frac{T - T_t}{1.4 * T_r}\right)^2 + 3.19 * \frac{T - T_t}{1.4 * T_r} + 0.5 \quad (2.6)$$

$$T_a < T_t \mid fr = 5 * \left(\frac{T - T_t}{1.4 * T_r}\right)^3 + 6.76 * \left(\frac{T - T_t}{1.4 * T_r}^2\right) + 3.19 * \frac{T - T_t}{1.4 * T_r} + 0.5 \quad (2.7)$$

The T_t and T_r parameters, default or calibrated, vary over the course of the year with sinusoidal functions, which are:

$$T_t = T_{ti} + T_{ti} * sin\left(\frac{month + 2}{1.91}\right) \quad (2.8)$$

$$T_r = T_{ri} * (0.55 + sin(month + 4)) * 0.6 \quad (2.9)$$

Where T_{ti} is the initial threshold temperature (default value is 2 °C) and T_{ri} is the initial transition temperature range (default value is 13 °C). To calibrate Kienzle a plot of daily T_a versus fr is required for the site in question from which values of T_{ti} and T_{ri} values can be estimated (Kienzle, 2008). Other empirical methods consider the diurnal T_a range (Leavesley *et al.,* 1983) and the T_a structure of the near surface atmospheric boundary layer (Gjertsen and Odegaard, 2005). The daily time step of most of these methods is a legacy of non-automated mountain weather stations with max-min thermometers and is less relevant with the advent of modern automated weather stations. The lack of high altitude weather stations with detailed observations of the precipitation phase in many parts of the world make phase-T_a calibrations, such as with Kienzle, impossible for most catchments. Further, these T_a proxies need to be recalibrated regularly to provide effective estimates as the climatic characteristics affecting the phase vary over time (Marks *et al.,* 2013) especially in the mountains of western North America (Mote *et al.,* 2005), which adds uncertainty to the application of these proxies in hydrologically non-stationary conditions (Milly *et al.,* 2008).

Other methods include observation of atmospheric humidity by use of other properties such as dew point (T_d) and thermodynamic wet bulb temperature (T_w) (Marks *et al.,* 2013). Marks *et al.* (2012) found that within a single precipitation event, the phase transition timing was better estimated by a 0 °C T_d threshold than by a 0 °C T_w or T_a threshold at Reynolds Creek, Idaho. A daily dataset at the Grove site (2056 m), in Reynolds Creek, from 1996 to 2008 showed insignificant differences in the fraction of precipitation as snowfall among T_a, T_d and T_w thresholds (Marks *et al.,* 2013). These differences in results between the long term and event scale suggest that there is temporal scale dependence to precipitation phase estimates and some dependence of phase on humidity (Marks *et al.,* 2013). The USGS Hydrological Simulation Program Fortran model empirically calculates a T_t that varies with T_a and T_d (Bicknell *et al.,* 1997). The method, hereafter referred to as HSPF, is:

$$T_t = T_{ti} + (T_a - T_d) * (0.12 + 0.008 * T_a) \quad (2.10)$$

Units for all variables in Equation 2.10 are in degrees Fahrenheit and T_{ti} is the initial temperature threshold (typically 31 to 33 °F or -0.5 to 0.5 °C). Although this model considers humidity, it does so empirically and so the spatial and temporal transferability of the model are uncertain. Empirical approaches can be used to identify phase but are limited in that they may not consider mixed precipitation (HSPF and T0), temporally variable meteorological conditions (HSPF, UBC and T0) and may be overly parameterised (Kienzle).

Studies comparing existing observations to phase methods demonstrate differences in their performance and errors. Feiccabrino and Lundberg (2008), found the best performance with polynomial relationships followed by double thresholds then single thresholds. By contrast, the temporally variable polynomial method of Kienzle (2008) was demonstrated to be superior but the error of the single threshold, double threshold and a complex algorithm integrating maximum and minimum T_a thresholds (as described by Leavesley *et al.,* 1983) were quite similar. The precipitation with misclassified phase varies between 7.1% and 9.6% for the Kienzle (2008) study and 3.2% to 11% for the Feiccabrino and Lundberg (2008) study. As the magnitude of these errors is large, the fact that the more advanced methods show only small improvements and the disagreement among the performance of methods by studies and sites all serve to demonstrate the difficulty and uncertainty associated with current approaches to identify precipitation phase with surface observations of T_a.

2.3 Psychrometric Relationships and Phase

The hydrometeor temperature (T_i) has a physical relationship with the phase of precipitation (Steinacker, 1983; Stewart, 1992; Sugaya, 1991). T_i is controlled by the surface energy fluxes which are governed by the energy and mass balance of the falling hydrometeor. The gradient of vapour pressure between a saturated surface, such as a hydrometeor, and an unsaturated air mass controls the rates of evaporation or sublimation. In contrast when the vapour pressure gradient reverses in saturated conditions, condensation may occur. Assuming adiabatic conditions in the atmosphere the latent heat flux will be balanced by the sensible heat flux and therefore a difference in temperature between the air and a saturated surface will exist. Adiabatic conditions are not always present particularly if there is a flux of net radiant energy to the hydrometeor. The psychrometrically controlled steady state relationship among T_a, T_d and T_i in unsaturated conditions is:

$$T_d < T_i < T_a \tag{2.11}$$

In saturated conditions the relationship is:

$$T_d = T_i = T_a \tag{2.12}$$

The saturation of the air is taken to be with respect to ice when the T_a is below 0 °C and with respect to water when T_a is above 0 °C. In regions with frequently saturated conditions, T_i and T_d follow T_a closely thus the differences between those methods that consider only T_a and those that also consider humidity will be small (Yamazaki, 2001; Fuchs, 2006). T_d or T_a methods are often applied to unsaturated conditions where they are invalid (Eq. 2.11). T_a methods cannot be physically based as they do not incorporate the effects of humidity on latent heat transfer (Stewart, 1992). Although T_d is a function of T_a and humidity, it describes the cooling necessary for an unsaturated parcel of air to reach saturation over constant pressure. T_d does not consider sensible and latent heat fluxes to the hydrometeor and thus does not correspond directly to T_i, though it can be used to improve empirical methods to estimate phase and has shown some success in this regard in one field study (Marks *et al.,* 2013).

T_i can be calculated using near-surface meteorological variables, T_a and relative humidity (RH), which are normally collected at weather stations. Any calculation from station level data presumes that the near-surface meteorology represents an equilibrium condition for the falling hydrometeor. Early methods of calculating the T_w, upon which calculations of T_i are based, used

a classic application of the coupled energy and mass balance with psychrometric charts, based on the existing understanding of the T_w depression developed by Carrier in the early 1900s (Gatley, 2004). Common calculation approaches since then have considered equations which require implicit solutions (Fuchs, 2006; Olsen, 2003) or over-simplified parameterisations (Yamazaki, 2001). Alternative solutions to quantify T_i are available as a result of the laboratory sublimation rate experiments of Thorpe and Mason (1966) which were modified by Schmidt (1972) and Pomeroy *et al.* (1993) for application to blowing snow particles moving in the atmosphere. Pomeroy and Gray (1995) conceptualised the mass balance of a sublimating hydrometeor as an ice sphere:

$$\frac{dm}{dt} = 2\pi r D Sh\left(\rho_{Ta} - \rho_{sat(Ts)}\right) \tag{2.13}$$

where dm is the change in mass [kg], dt is the change in time [s], r is hydrometeor radius [m], D is the diffusivity of water vapour in air [m^2 s^{-1}], Sh is the Sherwood number which is the ratio of convective and diffusive water vapour transfer from a particle surface to air, ρ_{Ta} is the water vapour density in the free atmosphere [kg m^{-3}] and $\rho_{sat(Ts)}$ is the saturated water vapour density at the hydrometeor surface [kg m^{-3}]. The energy balance of a sublimating ice sphere (Pomeroy and Gray, 1995) is:

$$L\left(\frac{dm}{dt}\right) = 2\pi r \lambda_t Nu(T_s - T_a) \tag{2.14}$$

where L is the latent heat of sublimation or vaporisation [J kg^{-1}], λ_t is the thermal conductivity of air [J m^{-1} s^{-1} K^{-1}], Nu is the Nusselt number which is the ratio of convective and conductive energy transfer from a particle surface to air, T_a is in [K] and T_s is the surface temperature of the hydrometeor [K]. Combining 2.13 and 2.14 gives:

$$L2\pi r D Sh\left(\rho_{Ta} - \rho_{sat(Ts)}\right) = 2\pi r \lambda_t Nu(T_s - T_a) \tag{2.15}$$

assuming $Nu = Sh$ for a blowing snow particle in a turbulent atmosphere (Lee, 1975) or a falling raindrop (Tardif and Rasmussen, 2010) and T_s is equal to T_i due to the large surface area/volume relationship and weak heat conduction within the hydrometeor (Chang and Davis (1974) and Watts and Farhi (1975) in Tardif and Rasmussen (2010)) then 2.15 simplifies to:

$$LD\left(\rho_{Ta} - \rho_{sat(Ti)}\right) = \lambda_t(T_i - T_a) \tag{2.16}$$

Rearranging 2.16 to solve for T_i gives:

$$T_i = T_a + \frac{D}{\lambda_t} L\left(\rho_{Ta} - \rho_{sat(Ti)}\right) \tag{2.17}$$

Solution of 2.17 can be achieved iteratively using methods such as the Newton–Raphston approach to increase the efficiency of solution. Following Thorpe and Mason (1966) D is estimated by:

$$D = 2.06 * 10^{-5} * \left(\frac{T_a}{273.15}\right)^{1.75} \tag{2.18}$$

Applying the ideal gas law ρ_{Ta} is quantified by:

$$\rho_{Ta} = \frac{m_w e_a}{\bar{R}\, T_a} \tag{2.19}$$

where m_w is the molecular weight of water 0.01801528 [kg mol^{-1}], $\bar{R}$ is the universal gas constant of 8.31441 [J mol^{-1} K^{-1}] and e_a is the actual vapour pressure [kPa]. The $\rho_{sat(Ti)}$ in Eq. 2.17 is calculated the same as ρ_{Ta} but uses T_i in place of T_a and assumes a RH of 100%. Care must be taken when calculating ρ as saturation vapour pressure varies if taken with respect to water (e_{satw}) when $T_a \geq 0\ ^\circ C$ or ice (e_{sati}) when $T_a < 0\ ^\circ C$. Following Dingman (2002):

$$e_{satw} = 0.611 e^{\frac{17.3 T_a}{237.3 + T_a}} \tag{2.20}$$

where T_a is in K. Following Buck (1981):

$$e_{sati} = 0.61115 e^{\frac{22.452 T_a}{272.55 + T_a}} \tag{2.21}$$

where T_a is in ° C. As RH is typically observed with respect to water, when $T_a \geq 0\ ^\circ C$, e_a is calculated by:

$$e_a = \frac{RH}{100} e_{satw} \tag{2.22}$$

and when $T_a < 0\ ^\circ C$ e_a is calculated by:

$$e_a = \frac{(RH/100)\, e_{satw}}{e_{sati}} e_{sati} \tag{2.23}$$

Following List (1949) λ_t is quantified by:

$$\lambda_t = 0.000063 * T_a + 0.00673 \tag{2.24}$$

L has a T_a dependency, thus for heat of sublimation (L_s, $T_a < 0°C$) (Rogers and Yau, 1989):

$$L_s = 1000(2834.1 - 0.29 T_a - 0.004 {T_a}^2) \tag{2.25}$$

and for heat of vaporisation (L_v,$T_a \geq 0°C$)

$$L_v = 1000(2501 - 2.361 T_a) \tag{2.26}$$

The depression of T_i relative to T_a is a function of T_a and RH (Figure 2.1 a). T_a and RH control the vapour density gradient between the atmosphere and the hydrometeor: T_a by varying the maximum vapour density (as a function of saturation vapour pressure) and RH by defining the vapour density deficit between the atmosphere and hydrometeor. The magnitude of D/λ_t [m^3 K kg^{-1}], termed the psychrometric exchange ratio, increases non-linearly with that of T_a (Figure 2.1 b) and quantifies the turbulent exchange of mass and energy between the atmosphere and hydrometeor. The form of Eq. 2.17 is similar to that of the thermodynamic T_w (Monteith and Unsworth, 2008).

$$T_w = T_a - \frac{1}{\gamma}\left(e_{sat(T_w)} - e_{T_a}\right) \tag{2.27}$$

Where γ is the psychrometric constant [~0.066 kPa K^{-1}] and $e_{sat(T_w)}$ and $e_{T_a}$are the vapour pressures for saturated conditions at T_w and actual vapour pressure at T_a. Two differences exist between Eq. 2.17 and Eq. 2.27. First, the degree of saturation is quantified with vapour pressure [kPa] for T_w rather than a specific humidity [kg m^{-3}] for T_i. Second, the exchange in heat and vapour transfer between a surface and the atmosphere is equated by γ for T_w and the psychrometric exchange ratio for T_i. The γ term directly relates the change in vapour pressure to a change in temperature. In contrast the psychrometric exchange ratio relates the change in water vapor to temperature as ratio of vapour and heat exchange, which are not equal and vary with temperature. This is similar to the concept of the modified psychrometric constant (γ^*), which considers the resistance ratio of vapour to heat diffusion between a surface and the atmosphere, and is used to quantify the measured T_w relative to the thermodyanimc T_w (Monteith and Unsworth, 2008). Calculation of γ^* follows Monteith and Unsworth (2008):

$$\gamma^* = \frac{R_V}{R_H}\gamma \approx 0.93\gamma \approx \frac{0.93\left(c_p p\right)}{\varepsilon L} \tag{2.28}$$

Where R_V is the resistance to vapour transfer, R_H is the resistance to heat transfer, c_p is the specific heat capacity of air [1.0035 kJ kg^{-1} K^{-1}], p is atmospheric pressure [kPa] and ε is the molecular ratio of water vapor to air [0.622]. In contrast to the psychrometric exchange ratio, which is a function of T_a, γ^* is a function of windspeed (Monteith and Unsworth, 2008). The difference between T_i and T_w (for both γ and γ^*) over a range of T_a and RH, Figure 2.2, shows that T_i will estimate colder temperatures than both the modified and unmodified T_w and that the difference increases with T_a.

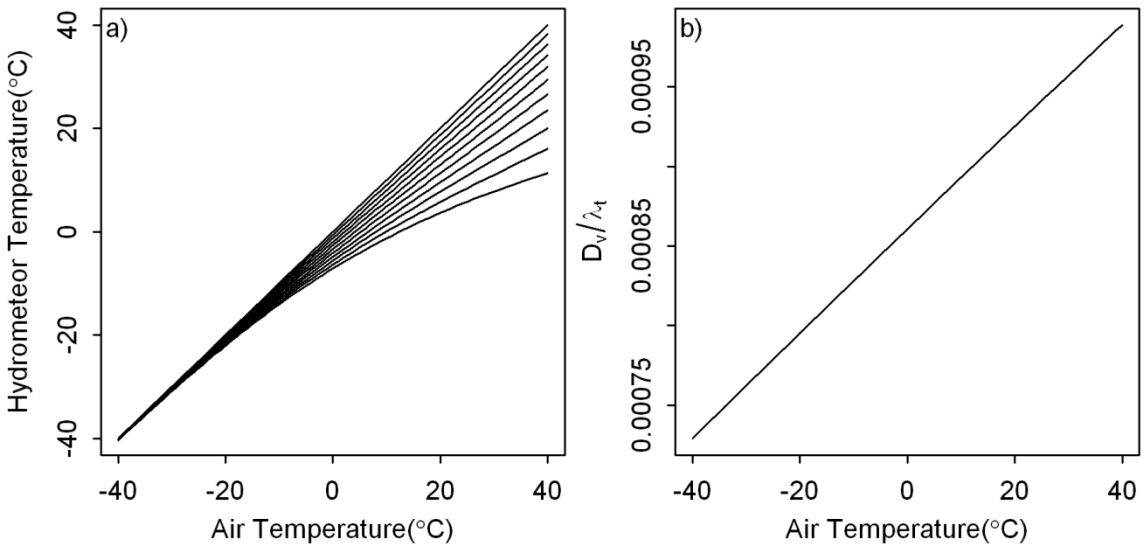

Figure 2.1: (a) Hydrometeor temperature (T_i) and (b) psychrometric exchange ratio (D/λ_t) is plotted versus air temperaure (T_a). The hydrometeor temperature (a) is plotted for values of relative humidity between 100% (straight line) and 0% in 10% increments.

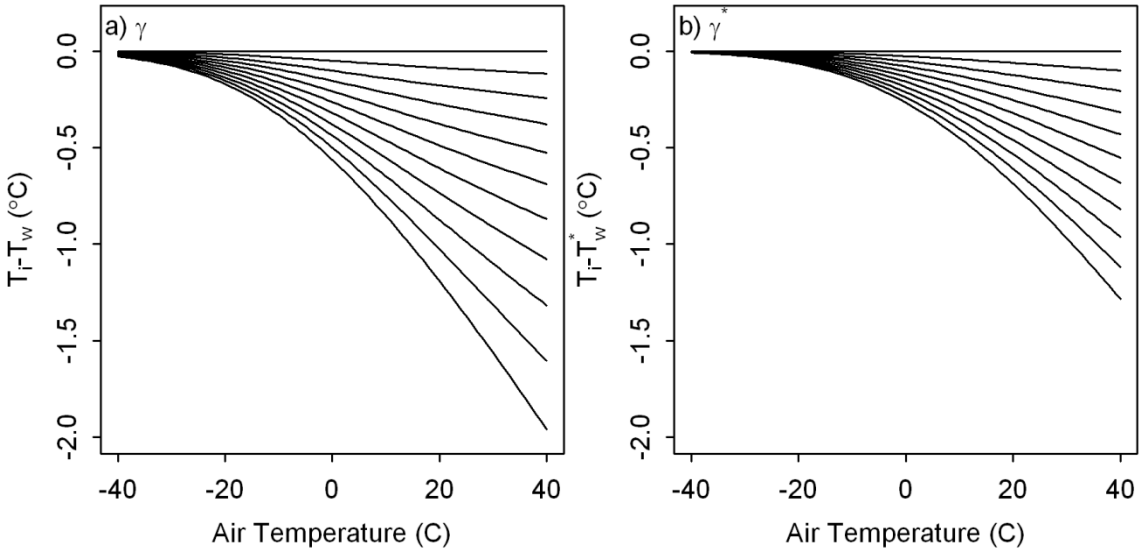

Figure 2.2: Difference between hydrometeor temperature (T_i) and (a) thermodynamic wet bulb temperature (T_w) and (b) wet bulb temperature with modified psychrometric constant (T_w^*) versus air temperature (T_a). The differences are plotted for values of relative humidity between 100% (straight line) and 0% in 10% increments.

The proposed T_i approach assumes thermodynamic equilibrium and insignificant net radiant energy to falling hydrometeors, which may not always be true (Schmidt, 1972). If a hydrometeor is falling through atmospheric layers of different properties the actual T_i can vary from T_i at thermodynamic equilibrium. The time lag for the hydrometeor to reach a new thermodynamic equilibrium T_i is a function of *RH*, ventilation and drop size and can vary between fractions of a second for cloud droplets to a few seconds for hydrometeors (Kinzer and Gunn, 1951). The time lag to reach thermodynamic equilibrium is ignored in this analysis as it is impossible to assess whether or not hydrometeors are in fact at thermodynamic equilibrium without profiles of atmospheric structure. In cases where the assumptions are invalid, the proposed calculation will overestimate T_i relative to actual conditions. Nevertheless the psychrometric energy balance should provide a more robust and more physically based index of precipitation phase than using T_a or T_d.

2.4 Hydrological Modeling and Phase Algorithms

The separation of precipitation into rainfall or snowfall is one of the most sensitive parameterisations in simulating cold region hydrological processes (Loth *et al.,* 1993). Studies of varying precipitation phase methods in hydrological models have focused almost exclusively on the effects on snowpack processes, the largest being changes in the depth and density of a snowpack (Loth *et al.,* 1993; Lynch-Stieglitz, 1994; Fassnacht and Soulis, 2002; Wen *et al.,* 2013). A common suggestion to reduce error is to use locally derived or calibrated T_a-phase relationships (Fassnacht and Soulis, 2002) but this is problematic in areas without precipitation phase observations. A consequence of using phase methods that do not reflect local conditions is that the consequent errors propagated in snowpack simulation are cumulative, which leads to systematic over or under-estimation of snow water equivalent (SWE) and depth that increase with time (Lynch-Stieglitz, 1994). In addition to changing the depth and density of a snowpack, varying the phase method causes errors in the calculated energy balance of a snowpack (Loth *et al.,* 1993; Fassnacht and Soulis, 2002). Overestimating the rainfall adds more energy to the snowpack by advection, increases the snowpack water content, leads to earlier ripening, increases latent heat transfer to the snow, reduces the albedo and increases the snow surface temperatures relative to reality (Loth *et al.,* 1993). Phase methods that define greater values of

the T_a thresholds (reducing the rainfall) result in less energy being transferred from the atmosphere into the snowpack leading to greater latent and ground heat fluxes to the atmosphere (Fassnacht and Soulis, 2002). Snowcover has a tremendous influence on land atmosphere interactions and thus changes in rainfall and snowfall cause land-atmosphere feedbacks (Wen *et al.,* 2013). Using greater values of T_a thresholds in a coupled atmospheric-land surface model simulates higher albedos, leading to cooler surface temperatures (Wen *et al.,* 2013). As a result the feedbacks that occur when coupling surface and atmospheric processes increase the sensitivity of snowcover properties to precipitation phase methods (Wen *et al.,* 2013). The translation of differences in snowcover due to different precipitation phase methods affects streamflow estimation in cold regions. Generally the greater the T_a threshold used, the larger and later will be the snowmelt streamflow peak (Fassnacht and Soulis, 2002).

2.5 Summary

The physical processes governing the phase of a hydrometeor at the ground surface are complex and common precipitation phase methods are oversimplifications of reality. The interaction of physical processes with meteorological patterns and terrain introduces phase uncertainty in even the most comprehensive atmospheric models (Minder *et al.,* 2011). Hydrology has often taken a more simplified approach and has focused on the available near surface data, rather than atmospheric model output, to identify phase. Over-reliance on T_a precipitation phase methods that lack a physical basis and spatial transferability has developed. In humid regions T_a precipitation phase methods can work well (as T_i and T_a are similar at saturation) but fail in sub-humid regions. Psychrometric approaches hold promise in being able to identify phase through the demonstrated physically-based relationship between phase and T_i.

CHAPTER 3. Psychrometric Energy Balance Phase Model Development

The development of a semi-physical psychrometric energy balance phase model is described in this chapter, which begins with a description of the site and data utilized and the quality assurance and control procedures followed. The first two objectives are addressed with a novel precipitation phase model and results pertaining to the temporal scale dependence and comparison with other empirical methods are presented. The chapter concludes with a discussion of the results.

3.1 Marmot Creek Research Basin

The data utilized in the analysis of the precipitation phase were collected in the Marmot Creek Research Basin (MC) by the University of Saskatchewan Centre for Hydrology which began installing instrumentation in 2005 (Pomeroy *et al.,* 2012). MC is situated in the Kananaskis Valley, Alberta, located approximately 70 km west of Calgary in the Front Ranges of the Canadian Rockies (Figure 3.1). The vegetation includes sparsely vegetated alpine tundra, alpine meadows and sub alpine and montane forests (Swanson *et al.,* 1986). The climate is dominated by long cold winters and cool wet summers. Mean daily T_a (1968-2012) at a mid elevation site (Upper Clearing: 1845m) ranges from 11.7 °C in July to -10.7 °C in January and is observed to be increasing (Harder *et al.,* 2013). Annual mean precipitation of 638 mm is recorded at the valley bottom and up to 1100 mm at upper elevations (Storr, 1967).

3.1.1 Hydrometeorological Observation Program

To estimate precipitation phase from field observations, reliable precipitation and other meteorological data are required at high temporal resolution. A comprehensive suite of hydrometeorological variables was obtained from weather stations that are regularly visited and maintained by field staff. The three automatic weather stations used in this analysis are the Hay Meadow (HM, large pasture in a valley bottom mixed-wood forest, 1436 m), Upper Clearing (UC, large clearing in coniferous forest, 1845 m), and Fisera Ridge (FR, alpine treeline site, 2325 m) stations. The observations considered in this study included T_a, RH, incoming and outgoing radiation, snow depth, total precipitation and tipping bucket rainfall. Observations have been taken every 10 seconds at UC since 2005, FR since 2007 and HM since 2008 with subsequent

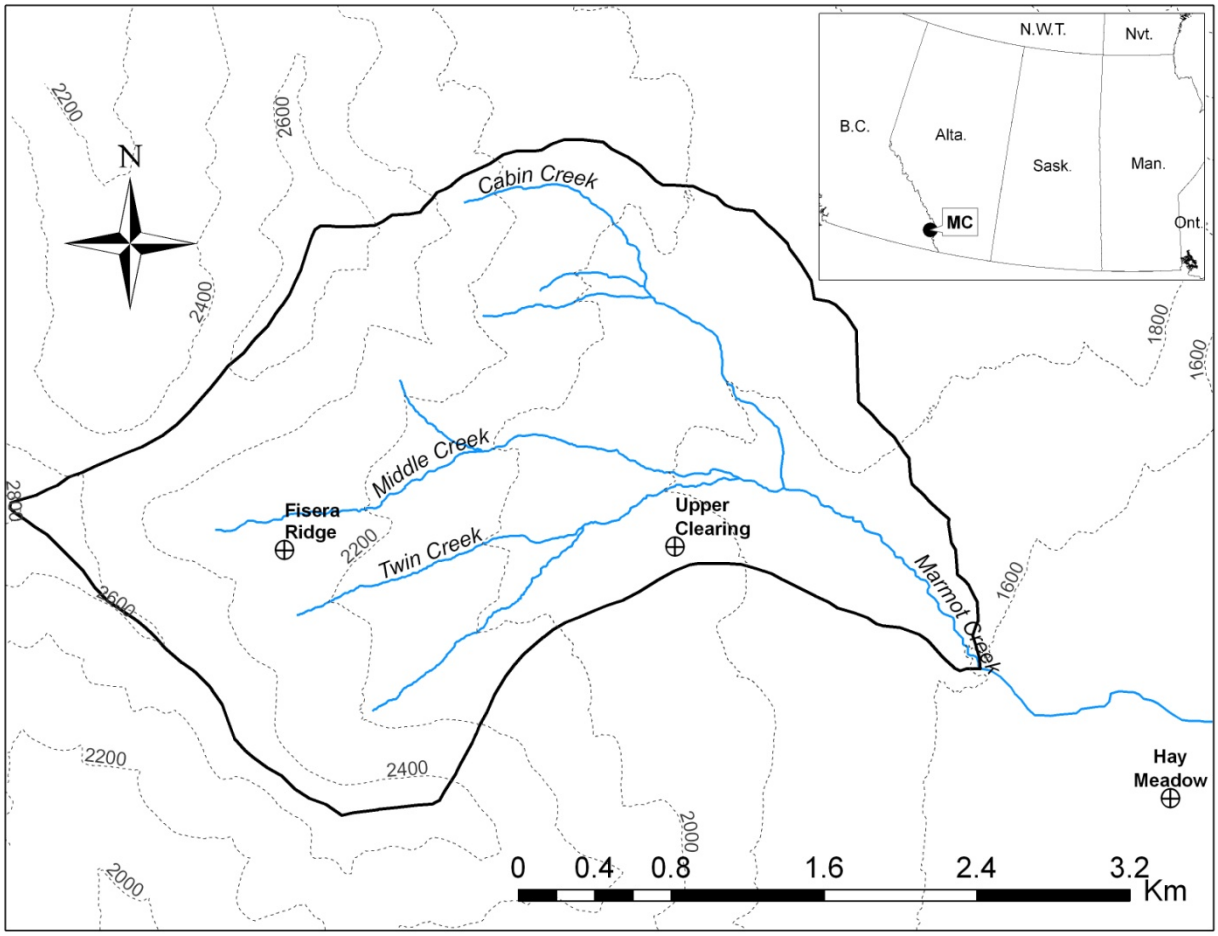

Figure 3.1: Marmot Creek Research Basin showing selected meteorological stations, basin boundary, mountain peaks and topographic contours and location in western Canada.

averaging to 15 minute intervals. Data up to July 9, 2012 were utilized in analysis. The Vaisala HMP probes utilize a thin film capacitive sensor whose dielectric properties are sensitive to relative humidity. The relative humidity is measured with respect to water with an operating range, appropriate to the study of precipitation phase change, between -20 °C and 60 °C (Anderson 1994). Total precipitation at all sites was measured with an Alter-shielded Geonor T-200B Series weighing gauge that uses a vibrating-wire weighing transducer to measure accumulated precipitation, but not phase. A mixture of anti-freeze and oil in the storage gauge inhibits the liquid in the gauge from freezing in the winter and reduces the evaporative losses in summer.

Data from a Meteorological Service of Canada weather station with automatic and manual observations at the Biogeoscience Institute Barrier Lake Field Station (BGSI), located 10 km east of MC, are used to provide an independent validation dataset for the daily timescale. A Nipher storage gauge and a Meteorological Service of Canada standard rain gauge are used to observe snowfall and rainfall manually in a small forested clearing. Nipher gauges consist of a copper cylinder surrounded by an inverted bell shaped shield to reduce wind induced undercatch errors (Goodison, 1978). Snow captured in the cylinder is melted after each observation interval and is then measured by a graduated cylinder. The Nipher snowfall was not corrected for wind effects as precipitation is only reported daily and appropriate wind speed data are unavailable.

Table 3.1: Marmot Creek Meteorological Stations and their Instrumentation

Site	Fisera Ridge (FR)	Upper Clearing (UC)	Hay Meadow (HM)	BGSI
Record length	10/2006- present*	6/2005- present*	7/2006- present*	1999- 2010
UTM (11U)	626107 5646559	628150 5646577	630742 5645259	637814 5654723
Elevation (m)	2325	1845	1436	1391
Variable				
T_a/ RH	Vaisala HMP45C212	Vaisala HMP35C	Vaisala HMP45C212	Vaisala HMP45CF
Outgoing and Incoming shortwave radiation	Kipp & Zonen CNR1[a]	LI-COR LI200S	Kipp & Zonen CNR1	n/a
Snow Depth	SR50	SR50	SR50-45	n/a
Rainfall	Hydrological Services TBRG[d] TB4	Hydrological Services TBRG TB4	Texas Electronics TE525M	MSC standard rain gauge
Total Precip. (rainfall & snowfall)	Geonor T-200B [b]	Geonor T-200B	Geonor T-200B [c]	Nipher Snow Gauge[e]

* data up to July 9, 2012 used in the analysis, [a] instrument added October 2007, [b] instrument added October 2008, [c] instrument added July 2005, [d] Tipping Bucket Rain Gauge, [e] Nipher gauge only observes snowfall

Systematic errors such as wetting losses are associated with Nipher snow gauges unlike the Geonor gauges within MC (Goodison, 1978). Reported precipitation phase is observed or estimated by the site observer who may or may not be observing the entire precipitation event, which is another source of uncertainty. Hourly T_a and RH, which are subsequently averaged to daily values, are measured separately at a site located approximately 100 meters to the northwest of the precipitation gauges in low brush. A summary of site instrumentation and data periods is given in Table 3.1.

3.1.2 Data Quality Assurance and Quality Control

Weighing precipitation gauge measurements have a high degree of precision, but may contain large systematic errors, and therefore must be carefully quality controlled to remove wind induced jitter effects and evaporative losses, as shown in Figure 3.2. A supervised data quality assurance and control procedure was instituted to remove obvious errors and noise from the Geonor precipitation datasets. The quality assurance and quality control procedure applied the following rules sequentially to the raw accumulated precipitation observations, the implications of these rules follow:

1. If changes in raw cumulative precipitation greater than 10 mm (very high and rare precipitation intensity) and less than 10 mm (an impossibly high rate for evaporative losses) occur over a 15 minute interval then the observation was removed.
2. If the raw accumulated precipitation observation was greater than 620 mm (the capacity of Geonor) it was removed.
3. All missing/removed accumulated observations were assumed to be equal to the last previous observed accumulated observation.
4. After removal of spurious data (1-2) and gap filling (3) differences of greater than 20 mm or less than -20 mm (the threshold being determined by trial and error) in adjacent values the 15 minute accumulated precipitation data were assumed to be due to emptying or recharging of Geonor liquid and these differences were removed to form a continuous accumulated precipitation record.
5. Removal of data during problematic time periods, e.g. damaged sensor, power or datalogger failure.

6. Jitter was removed from accumulated precipitation through application of a rolling maximum, where a cumulative precipitation observation is only retained if greater than the previous maximum observed cumulative precipitation.
7. Supervised correction of gauge evaporative losses.

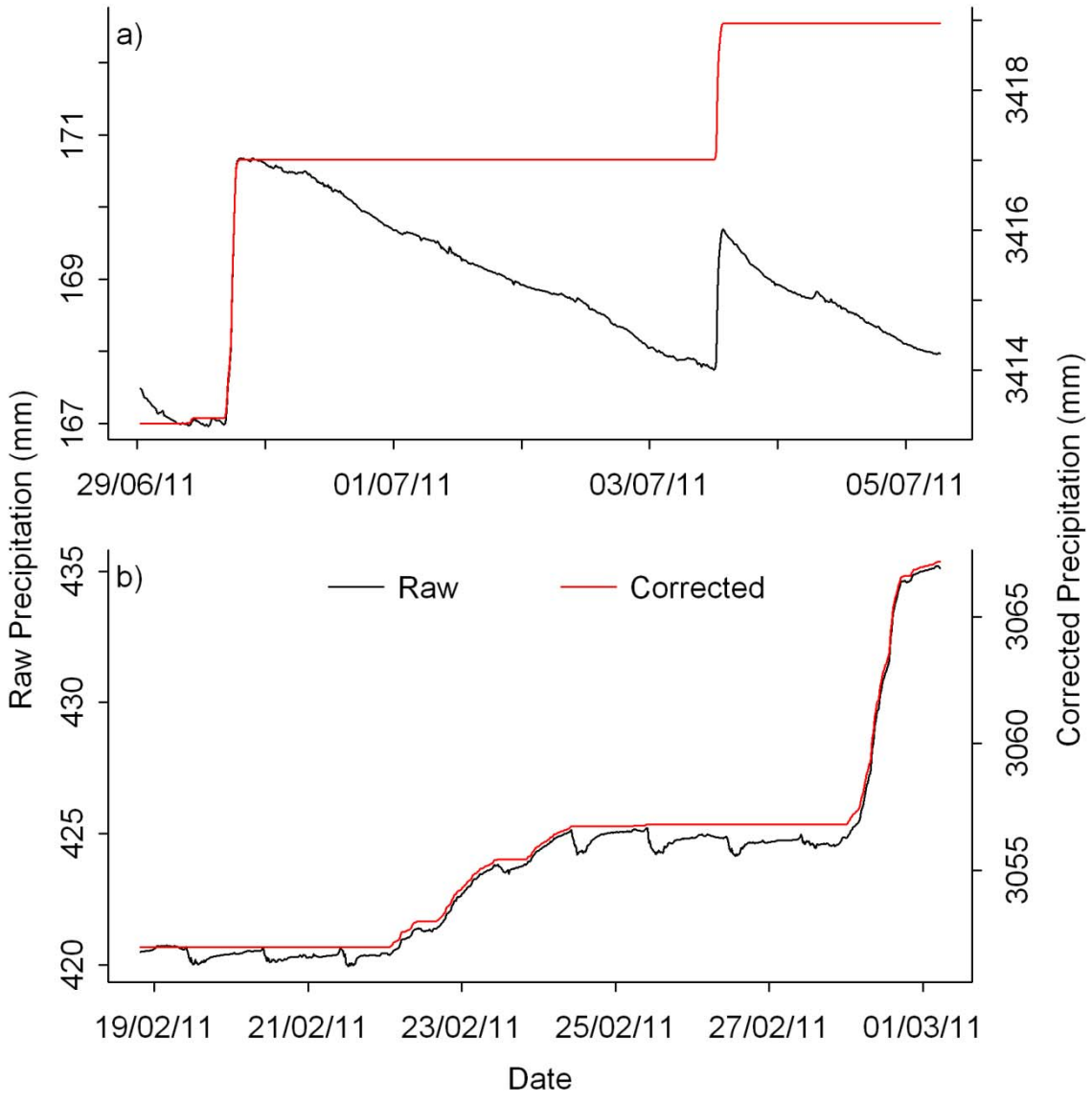

Figure 3.2: Examples of Upper Clearing raw and corrected cumulative precipitation from Geonor T-200B weighing gauge. (a) Significant evaporation (manual correction of 1.95 mm over four day period) with negligible jitter and (b) diurnal variability (no correction) with minor jitter.

The rolling maximum filter is intended to remove all remaining jitter from the dataset. It operates by retaining a cumulative precipitation observation for a time step only if it is greater than the previous maximum observed cumulative precipitation. Otherwise the previous maximum is assumed to be the cumulative precipitation. The rolling maximum works well in that it preserves the cumulative change and the timing of precipitation events. Unfortunately in the presence of evaporative losses (Figure 3.2a) the rolling maximum can mask precipitation events if the total evaporation is larger than the subsequent precipitation event. In addition, the filter may not catch the precise start of a precipitation event as precipitation must first exceed the rolling maximum which can take several time steps with precipitation. A rolling maximum filter by itself introduces a bias to underestimate precipitation. An intercomparison of the auto-filtered and raw data was employed to identify erroneous departures between the two datasets. These departures were then corrected by manually replacing the auto-filtered accumulated precipitation data with the actual change from the raw data. These corrections were usually implemented to capture the beginning of precipitation events especially when there was a long interval between events during which evaporation effects became important.

Other procedures to remove noise and fill gaps in Geonor precipitation are available including those suggested by Nayak *et al.* (2008) which corrects precipitation by comparing low and high frequency noise and of Lamb and Durocher (2004) who present noise threshold and filter methods. The final purpose of the precipitation data dictates which correction method should be utilized. Thus the uncertainties that the Nayak *et al.* (2008) and Lamb and Durocher (2004) methods introduce by either shifting timing of precipitation or omitting evaporative losses makes them inappropriate for this analysis. The correct timing of precipitation events and the amount for each interval is deemed to be more important than imputing values for missing observation intervals.

3.1.3 Phase Identification

With the development of a high temporal resolution precipitation dataset it was then possible to identify the precipitation phase by using the suite of other hydrometeorological variables. Following the determination of phase, the Geonor precipitation identified as snowfall was corrected for wind induced gauge undercatch. Deformation of the wind field over a gauge orifice causes displacement and acceleration of snow particles leading to an undercatch in recorded

snowfall (Thériault *et al.,* 2012). The snowfall was corrected for wind undercatch using the algorithm developed for Alter-shielded Geonor gauges by MacDonald and Pomeroy (2007). In theory, only concurrent observations from a total (liquid and solid) precipitation gauge and tipping bucket rain gauge (only liquid) are required to identify phase, however in practice these measurements are too uncertain to be used exclusively. Error in the timing of rainfall from tipping bucket rain gauges (TBRG) in cold weather mean that rainfall observations alone cannot be used to determine precipitation phase. Therefore, phase was manually identified for each 15 minute measurement of precipitation from the Geonor using measurements of rainfall T_a, RH, albedo (outgoing/incoming shortwave radiation), and snow depth. Identification of precipitation phase was limited to solid or liquid phase and did not identify mixed phase. Confidence in phase identification was increased when observations from more than one instrument indicated agreement on the phase. The general approach employed the following logic:

- Geonor Weighing Gauge: is a cumulative record of rainfall and snowfall events. Geonor precipitation (corrected for wind induced undercatch using the method of MacDonald and Pomeroy (2007)) is assumed to be the true amount of precipitation relative to TBRG and so phase was only identified if the Geonor recorded precipitation.
- Tipping Bucket Rain Gauge: is a measure of the amount of liquid precipitation during an interval. Rainfall was identified if the TBRG and Geonor recorded precipitation in approximately the same magnitude and timing. Snowfall was identified if a TBRG event occurred after a Geonor precipitation event and if the TBRG event was determined to be due to melt of snow accumulation in the gauge orifice due to either the solar heating of the instrument or an increase in T_a.
- Albedo: Rainfall was identified if the magnitude of the albedo was small (0.1-0.2 over bare ground and < 0.6 for rainfall on a snowpack) or decreasing. Snowfall was identified if the albedo was greater than 0.8. When the calculated albedo exceeded 1.0 it was assumed that this was due to snowfall covering the incoming radiometer.
- Snow Depth: an ultrasonic depth gauge (Campbell Scientific Canada SR50) was used to measure distance to the surface (ground or snowpack surface). An increase in snow depth was used to identify snowfall, while no change or a decrease in snow depth was used to identify rainfall.

As an example of the uncertainty in tipping bucket rain gauge observations of rainfall and the usefulness of other meteorological variables to estimating phase, a mixed-phase precipitation event starting September 16, 2010 is shown in Figure 3.3. The accumulated total precipitation from the Geonor weighing gauge (black line) shows a 20 mm event spanning from the early morning of September 16, 2010 to noon September 17, 2010. The tipping bucket (blue line) recorded low intensity rainfall during September 16th that was smaller in accumulation than the higher intensity precipitation observed by the Geonor and then a large accumulation, high intensity event, on the afternoon of the 17th (after the event as described by the Geonor has ended). From the difference in TBRG and Geonor it can be inferred that the precipitation event began as rainfall but that the phase changed to snow throughout the 16th and the spike in the tipping bucket rain gauge was actually caused by snow melting in the orifice of the tipping bucket gauge. In this event, the snow depth (black dots) confirms the occurrence of snowfall due to the observed snowpack accumulation but due to scatter in the observations, the actual point of phase change cannot be determined from the snow depth observations. Using the albedo observations (red line) the phase change is clearly identified as occurring when the albedo jumped from 0.2 to 1.0 at 15:45 on September 16th. The increase in albedo coincides with fresh snow on the ground, or more likely, the incoming radiometer being covered by fresh snowfall. The observations available do not provide information on fraction of rain or snow in the same interval, mixed phase is not identified and is assumed to negligible. By using the four available instruments, the phase of the precipitation was determined and the time of the phase change was identified.

The phase of precipitation was identified at the UC, FR and HM sites from 2005 to 2012 (Figure 3.1). Personal judgment, considering seasonal trends, patterns and timing in the observations, was required in some situations when the sensor behaviour was unclear or contradictory. The longest and highest quality dataset was UC, which was used to develop the T_i phase relationship; HM and FR had shorter usable records due to their missing data and were only used for verification. At the HM and FR sites, phase identification primarily relied on observations of albedo and snow depth, which were the most reliable indicators of phase as the TBRG observations were intermittent at FR due to the harsher environment and were highly unreliable at HM due to rodent damage. The greatest source of error in this analysis is in the manual

determination of phase but this is considered negligible because of the redundancy due to the use of multiple sensors and because the cumulative errors are small on 15 minute intervals.

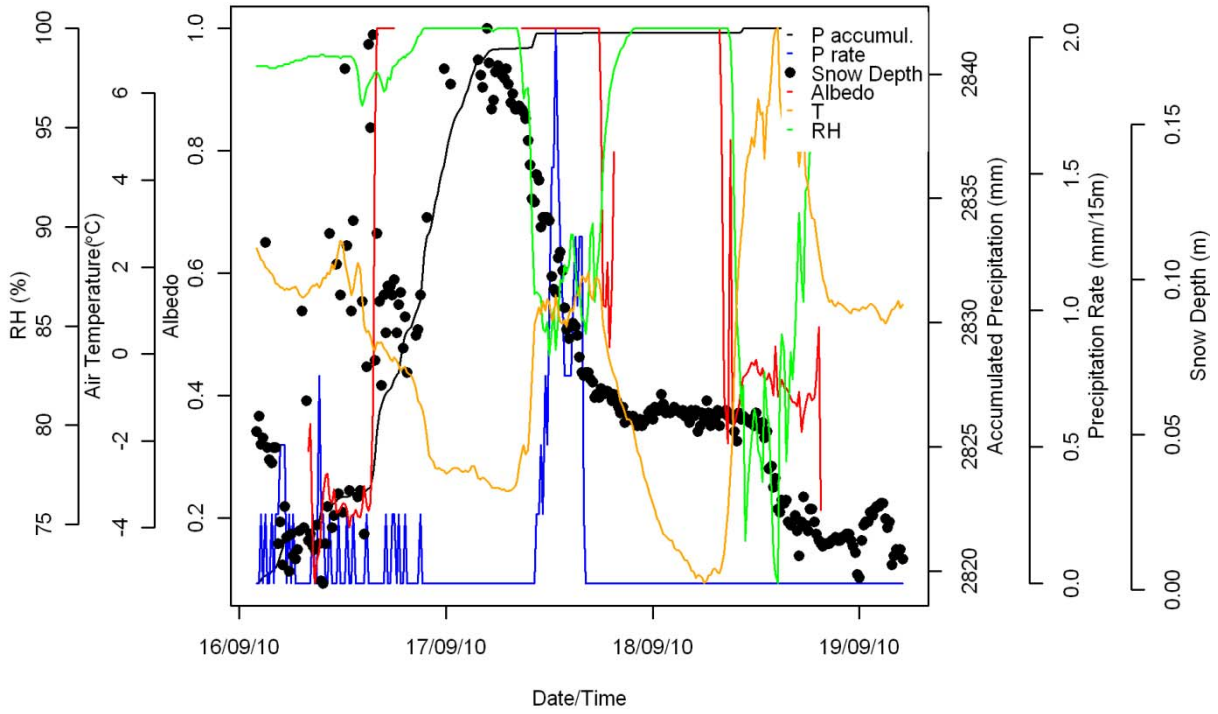

Figure 3.3: Meteorological data used to identify precipitation phase.

3.2 Analysis and Results

3.2.1 Temporal Scale dependence of Hydrometeor Temperature and Phase

To demonstrate the temporal scale dependence of precipitation phase with respect to T_a and T_i cumulative snowfall and rainfall at UC are plotted as histograms for T_a and T_i (Figure 3.4). It is apparent that the mode of the precipitation occurs at air temperatures near 0 °C indicating the importance of accurate phase determination at this site. Temporal scale dependence is evident when comparing the 15 minute (Figure 3.4 a and c) and daily time intervals (Figure 3.4 b and d). The transition range is greater for the daily interval than the 15 minute interval as the number of bins having total rainfalls and snowfalls greater than 5 mm is 4 for the 15 minute interval data (Figure 3.4a) versus 7 for the daily interval data (Figure 3.4b) for T_i. A similar pattern is observed for T_a (Figure 3.4 c and d). In addition the 15 minute interval T_i has a smaller transition range than T_a, number of bins having total rainfalls and snowfalls greater than 5 mm is 4 for T_i (Figure 3.4a) versus 6 for T_a (Figure 3.4). The 5 mm threshold is selected to avoid the

cumulative effects of hydrologically insignificant events. Therefore observations available to estimate the precipitation phase require a phase determination methodology that can take into account the effects of the time scale. The range of phase uncertainty is a function of time interval and type of temperature observation, suggesting that the T_i, especially for shorter time scales, should be a better predictor of precipitation phase than T_a.

A Kolmogorov-Smirnov (KS) test, which is a non-parametric test to determine if two samples come from the same distribution, compared the 15 minute, hourly and daily data sets (Table 3.2). A significance criterion of $p \leq 0.05$ was used. The 15 minute and hourly rainfall distributions were statistically similar but were different from the daily distribution. In contrast the comparison of snowfall distributions between timescales were all observed to be significantly different distributions.

Snowfall and rainfall histograms were plotted with respect to the T_i and T_a from the UC dataset for large and small events (Figure 3.5). The amount of precipitation in an event influences the importance of the hydrological response to the precipitation input; thus an understanding of the temporal scale dependence of large and small events is important. By categorizing the dataset by precipitation event sizes it is shown that the phase transition range narrows for large events (Figure 3.5). The number of 1 °C bins with more than one rain and snow event varied between 14 and 15 for the small events (Figure 3.5 a, c and e) and between 4 and 5 for the large events (Figure 3.5 b, d and f). Less error can be expected in the identification of the precipitation phase of larger precipitation events.

Table 3.2: Kolmogorov-Smirnov p values of hydrometeor temperature (T_i) histograms

	Rainfall		Snowfall	
Time Interval	1 Hour	15 Minute	1 Hour	15 Minute
Daily	0.04	0.01	0.00	0.00
1 Hour		0.47		0.03

$p \leq 0.05$ means distributions are significantly different

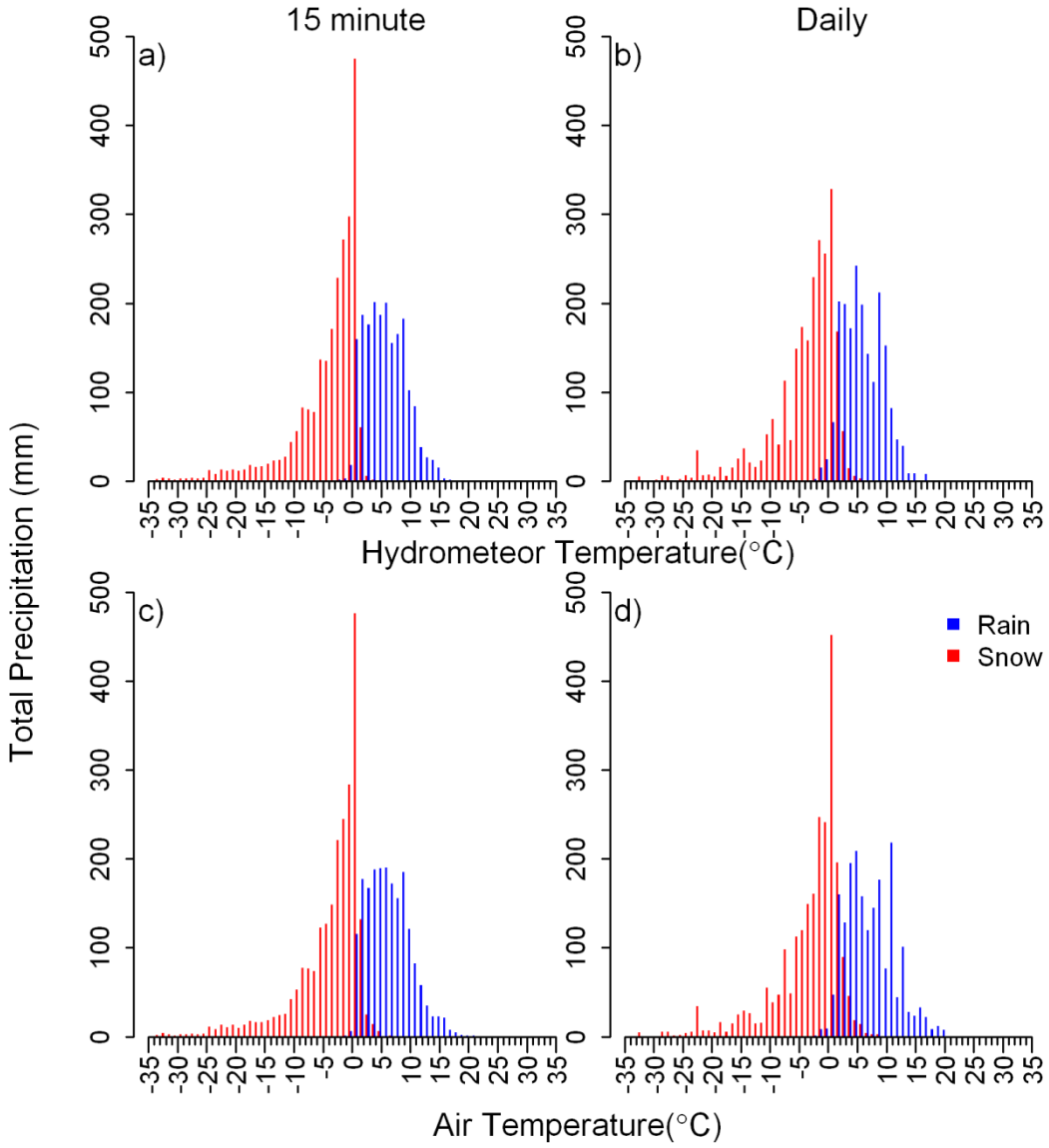

Figure 3.4: Total snowfall and rainfall histograms for the (a and c) 15 minute and (b and d) daily time intervals for (a and b) hydrometeor (T_i) and (c and d) air temperatures (T_a) at Upper Clearing for 2005-2011.

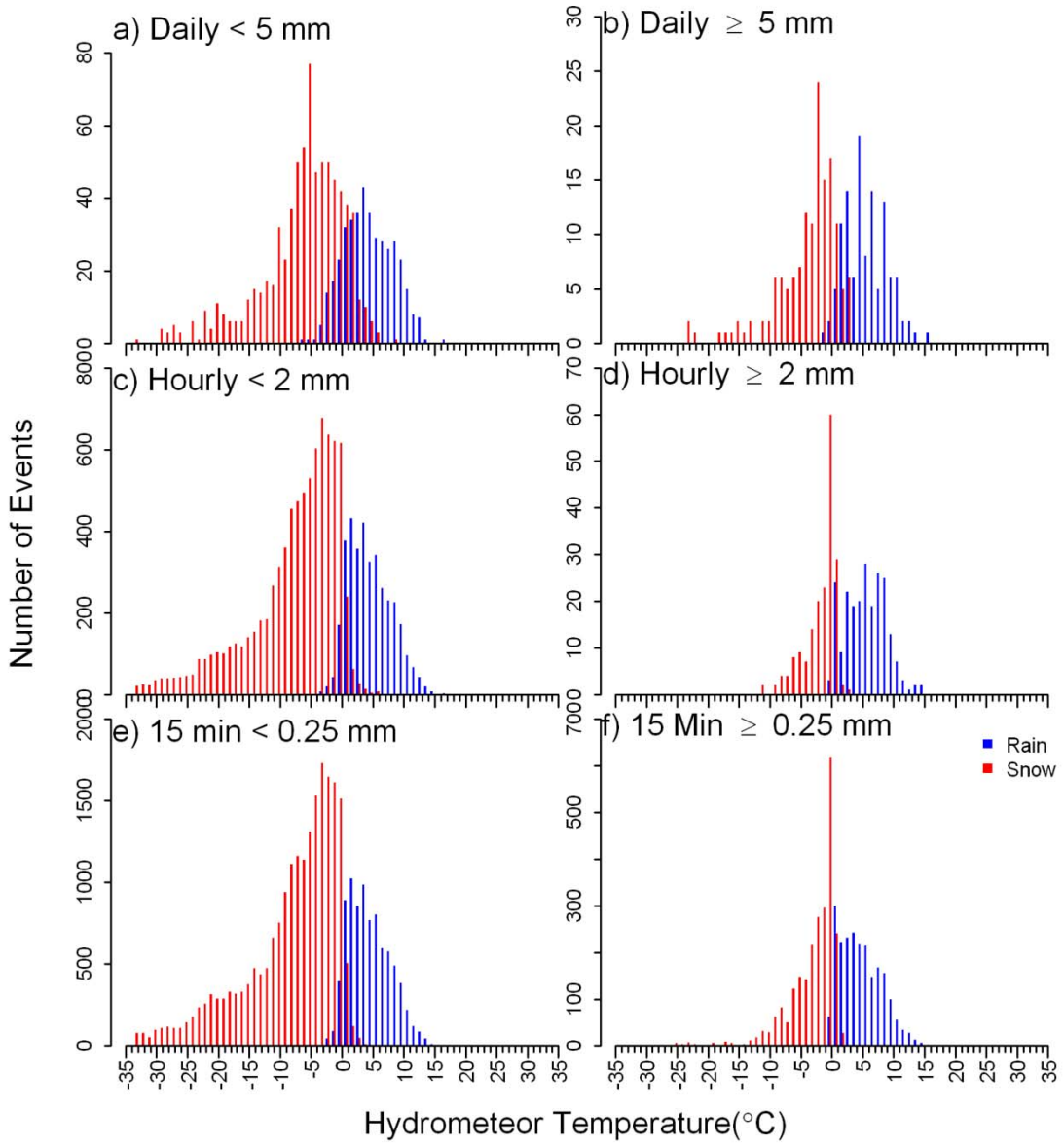

Figure 3.5: Histograms of hydrometeor temperature (T_i) versus precipitation phase for small (a < 5 mm, c < 2 mm and e < 0.25 mm) and large (b ≥ 5 mm, d ≥ 2 mm and f ≥ 0.25 mm) events on the (a and b) daily, (c and d) hourly and (e and f) 15 minute time intervals at Upper Clearing for 2005-2011.

3.2.2 Hydrometeor Temperature and Precipitation Phase Relationship

Figures 3.4 and 3.5 show that in the case of the sample datasets there is no distinct phase change measured at $T_i = 0$ and so no strictly physical calculation of phase is possible using Equation 2.17. The T_i transition range is due to variability in local precipitation and meteorological conditions over the observation intervals, lack of thermodynamic equilibrium in falling hydrometeors, errors in physical understanding and/or measurement errors. To relate the T_i to precipitation phase while taking into account these uncertainties, the fraction of precipitation as rainfall, f_r, was calculated from UC observations for each 0.1 °C T_i increment. Rainfall fraction is expressed as:

$$f_r(T_i) = \frac{\sum_{T_i} rainfall(mm)}{\sum_{T_i} rainfall(mm) + \sum_{T_i} snowfall(mm)} \tag{3.1}$$

where T_i is the mean temperature of each 0.1 °C T_i increment. The shape of the measured relationship between T_i and the rainfall fraction, f_r, appeared to be sigmoidal and so was fitted to the following function:

$$f_r(T_i) = \frac{1}{1 + b * c^{T_i}} \tag{3.2}$$

where b and c are coefficients and T_i is the hydrometeor temperature defined in Equation 2.17.

The rainfall ratios versus T_i at UC for 2005 to 2011 are used to fit Equation 3.2 curves with a nonlinear least square approach, using the nls function in R, over five time intervals as plotted in Figure 3.6. The proposed semi-physical model was fitted using the UC dataset and then validated with the FR and HM datasets at 15 minute, hourly and daily time intervals. The BGSI dataset was included in the validation of the daily time interval. Performance was assessed with the root mean square difference (RMSD) and mean bias (MB):

$$RMSD = \sqrt{\frac{\sum(X_s - X_o)^2}{n}} \tag{3.3}$$

$$MB = \frac{\sum X_s}{\sum X_o} - 1 \tag{3.4}$$

Where X_o and X_s are observed and simulated values and n is the number of values. The RMSD is a weighted measure of the difference between observation and simulation and has the same units as the observed and simulated values. The MB indicates the ability of the relationship to

identify precipitation phase; positive or negative values of MB imply systematic over prediction or under prediction, respectively, of simulated values with respect to observations. The values of b and c and the RMSD and MB for each relationship are presented in Figure 3.6. The T_i transition range and scatter increases with the time interval. The same methodology was used to fit curves with respect to T_a (Figure 3.7) to see if T_i, which varies with degree of saturation, makes any difference in partitioning precipitation as most precipitation events occur in saturated or near saturated conditions. The T_i relationships are stronger at all timescales analyzed as they have lower RMSD and MB values than the T_a relationships. Combining Equation 2.17 and Equation 3.2 yields a semi-physical relationship for the rainfall ratio that relies on the psychrometric energy balance calculation of T_i and fitting to adjust for scatter due to time scale, observation error, deviation from thermodynamic equilibrium assumptions and other factors. The proposed model is hereafter referred to as PSY. Although PSY is fitted to measured data, its physical basis should provide robustness in application to other environments and the temporal scale dependence of the model is useful in applying it to observations at differing intervals.

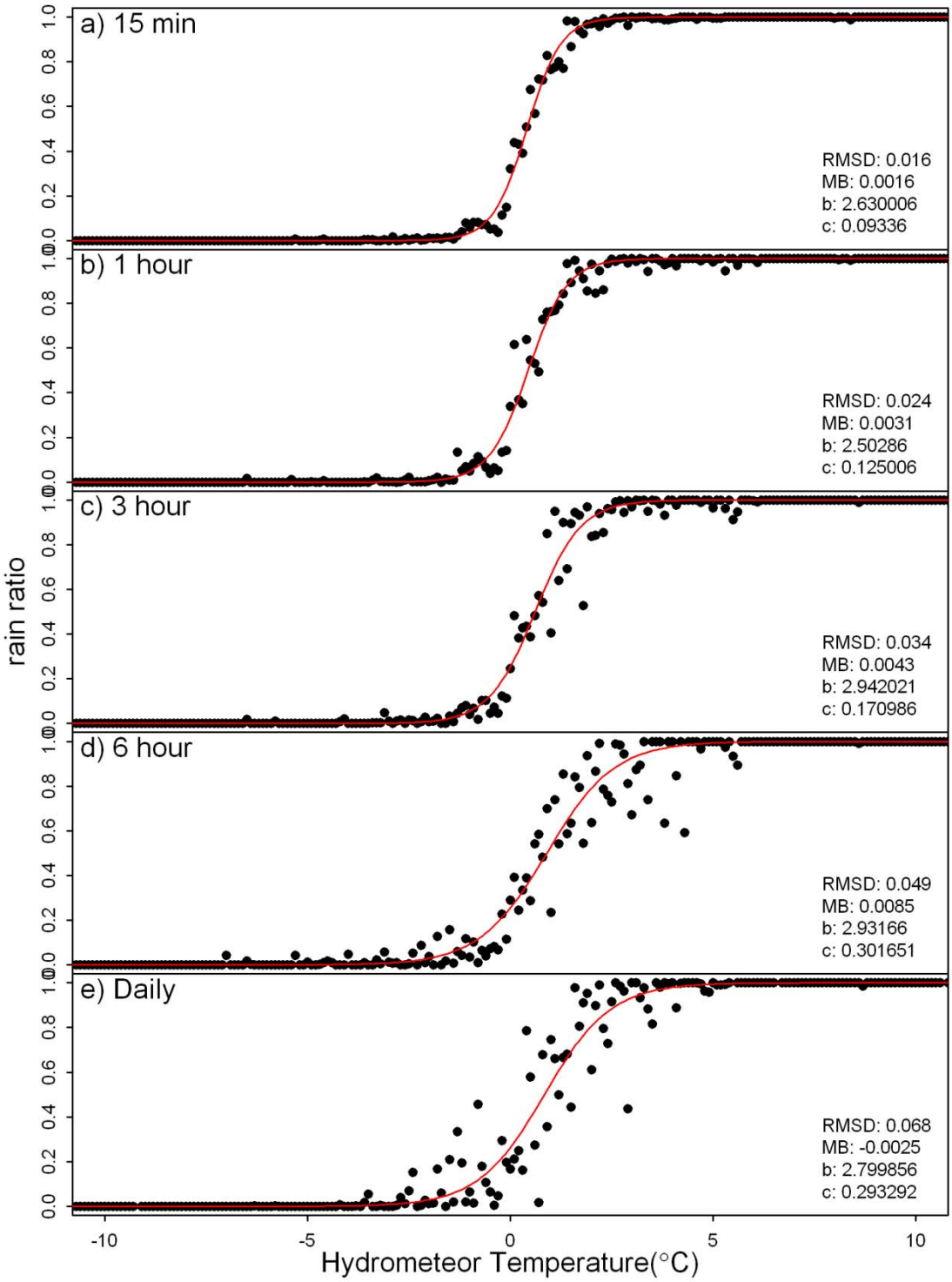

Figure 3.6: Hydrometeor temperature (T_i) and precipitation phase for the Upper Clearing (2005-2011) and the root mean square difference (RMSD) and mean bias (MB) of the fitted relationship for (a) 15 minute, (b) hourly, (c) 3 hour, (d) 6 hour and (e) daily time scales.

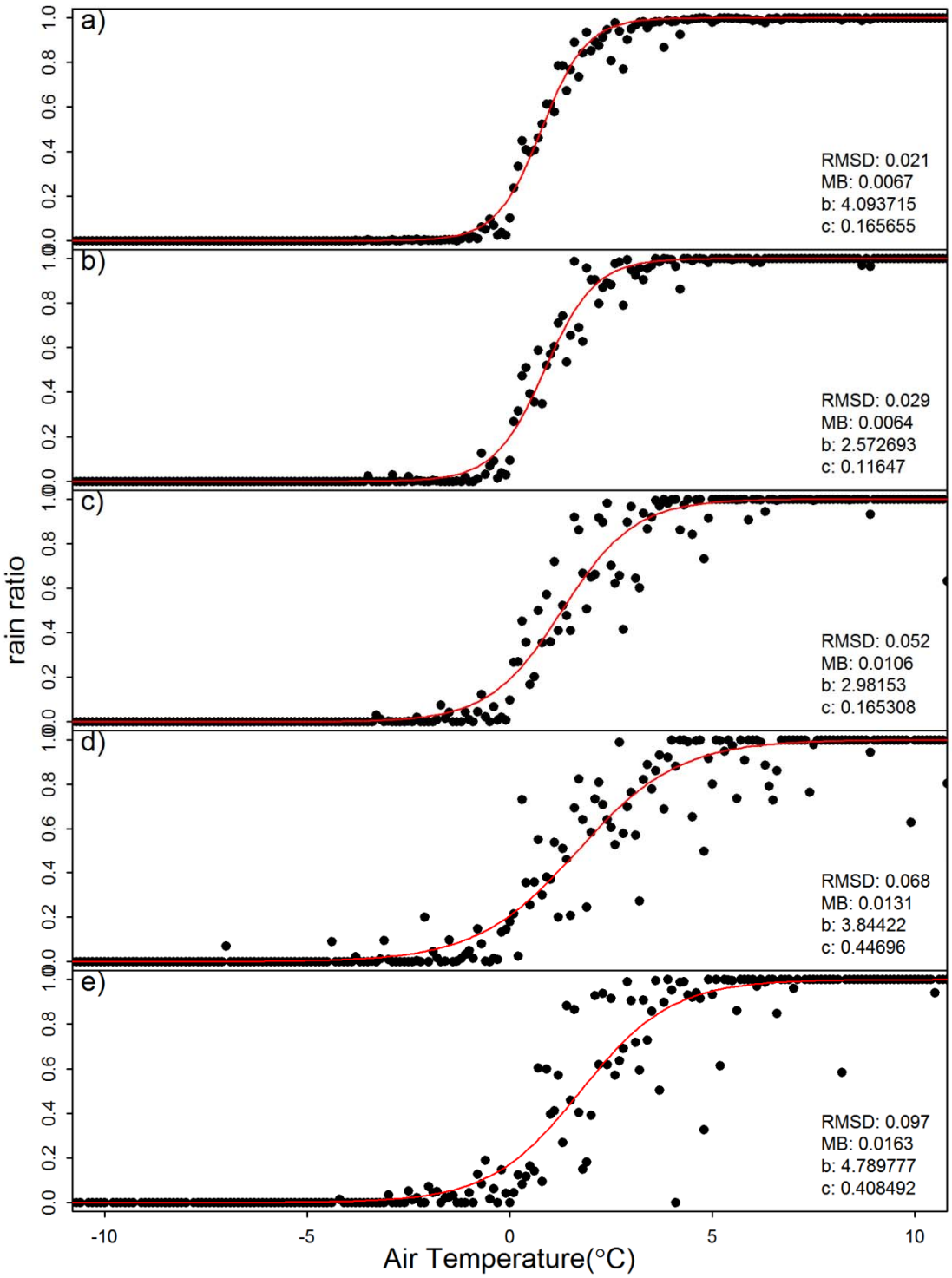

Figure 3.7: Air temperature (T_a) and precipitation phase for the Upper Clearing (2005-2011) and the root mean square difference (RMSD) and mean bias (MB) of the fitted relationship for (a) 15 minute, (b) hourly, (c) 3 hour, (d) 6 hour and (e) daily time scales.

3.2.3 Phase Method Intercomparison

The proposed semi-physical psychrometric energy balance relationship fitted to UC (Equation 3.2) was tested and compared to the other hydrological approaches for phase estimation, described in the literature review (T0, UBC, HSPF and Kienzle), using observations from FR, HM and BGSI. An additional method utilising a single T_i threshold ($T_t = 0°C\ T_i$) is included and is hereafter referred to as Ti0. The validation of the proposed method at FR (high elevation) and HM (low elevation) sites tested the performance of phase partitioning methods at varying elevations, and the use of the BGSI data tested the relationships outside of the research basin. All of the comparison methods were originally developed for the daily time scale, making application to sub-daily timescales potentially problematic. All methods were employed on daily, hourly and 15-minute time steps. PSY is temporally scale dependent thus the b and c parameters were varied for each time step length.

The RMSD and MB statistics for the modelled phase methods are shown for calibration datasets in Figure 3.8 and validation datasets in Figure 3.9. With the exception of Kienzle_adj and PSY, which were fitted to UC data, all other methods used default values of their parameters. The calibration comparison results, plotted in Figure 3.8, show that the semi-physical PSY method works best for daily time scales. At hourly intervals, the Kienzle methods worked equally well, with Kienzle_adj showing slightly better scores for RMSD and the Kienzle having a better MB. For the 15 minute scale the semi-physical PSY method worked best, showing better scores for RMSD and the Kienzle having slightly better MB values. Kienzle can have better performance than the calibrated Kienzle_adj as fitted parameters are determined visually from a plot rather than through a formal calibration technique that optimises an objective function. The weak physical basis of the T_a-phase relationship makes Kienzle and its calibration approach inconsistent and unreliable. Assessing the performance of the method across time scales is not possible for RMSD as varying the time interval changes the properties of the dataset. Decreasing the time interval leads to a larger sample size, more time steps, and a smaller error for each time interval; less precipitation in smaller time intervals reduces the error. However, the MB values are comparable between time scales.

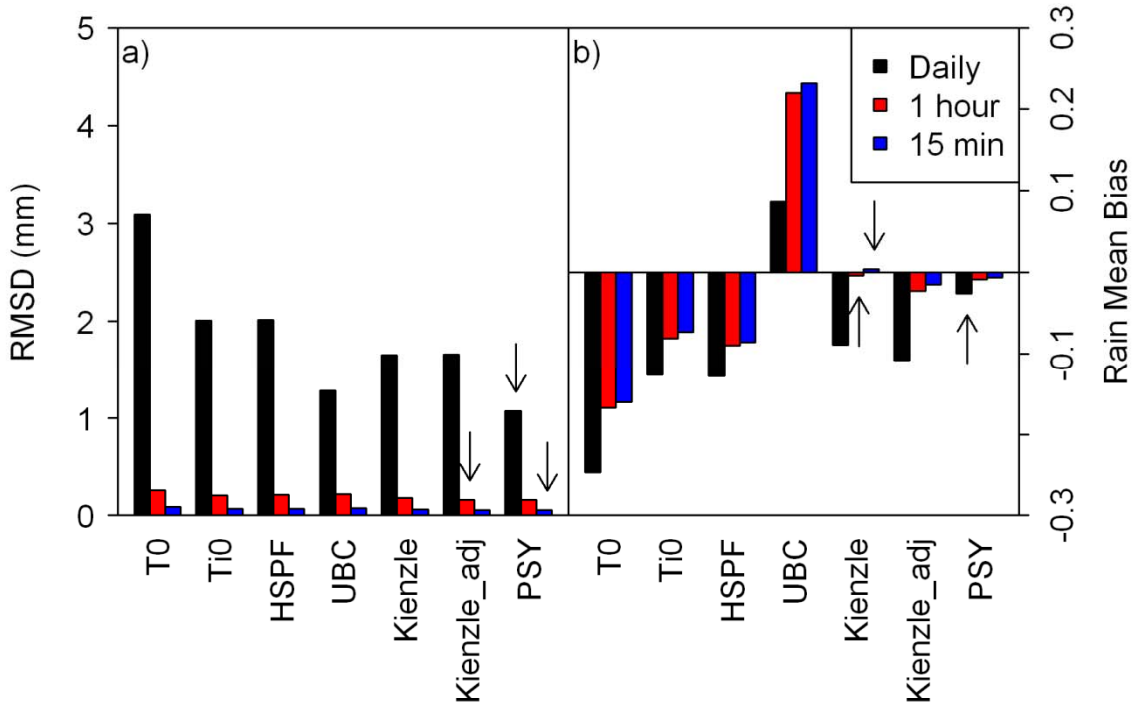

Figure 3.8: Precipitation phase determination methods intercomparison at calibration site (UC) with statistics against observations showing (a) root mean square difference (RMSD) and (b) mean bias (MB). The best result for each time interval and test is denoted by an arrow.

The comparison of phase partitioning methods plotted in Figure 3.9 shows that Kienzle_adj and PSY perform better using calibration than without. On the daily time interval UBC was most accurate, though its MB performance degraded over shorter time intervals. The failure of the UBC method on the sub-daily scale illustrates the sensitivity of phase identification to the time interval. The UBC method fails when the observed transition range narrows, for the sub-daily time intervals. Omitting UBC due to its degraded performance at short time intervals, the semi-physical PSY model is the most accurate model for the daily and hourly intervals, showing that its physical basis provides a robustness that transcends site characteristics, time scales and minor calibration.

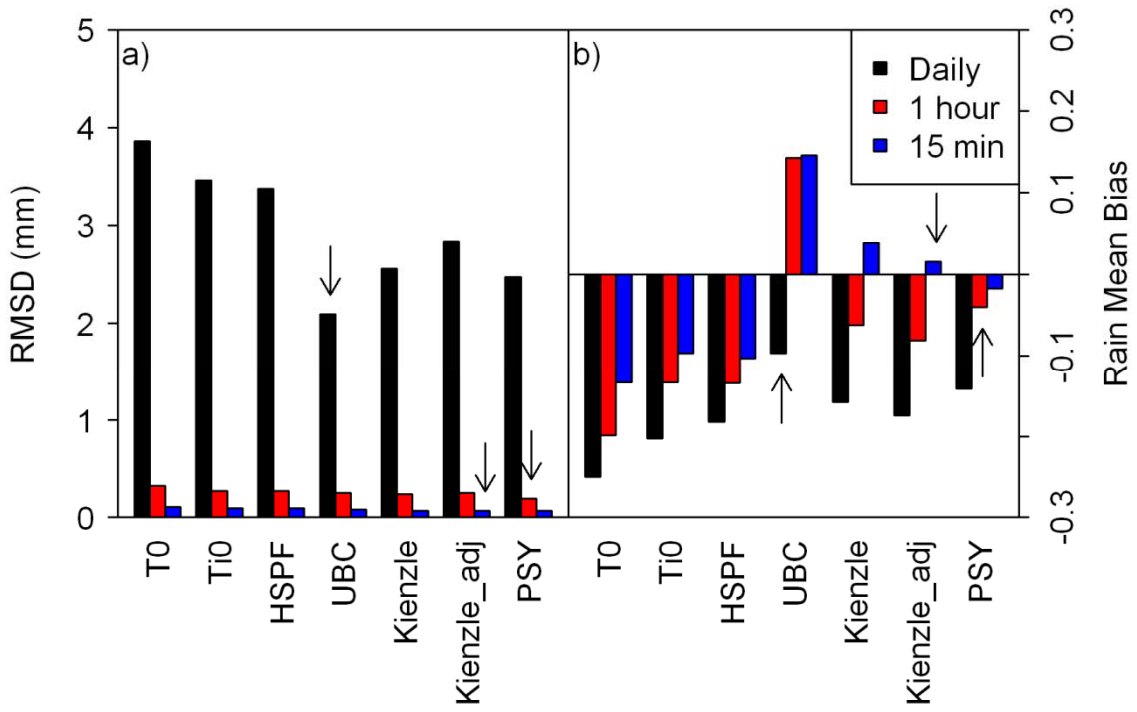

Figure 3.9: Precipitation phase determination methods intercomparison at validation sites (FR, HM and KFS) with statistics against observations showing (a) root mean square difference (RMSD) and (b) mean bias (MB). The best result for each time interval and test is denoted by an arrow.

3.3 Discussion

3.3.1 Precipitation Phase Dynamics

The temporal scale dependence of precipitation affects its estimation. Over 15 minute intervals the mixed-phase transition ranges are quite small, being 2.9 °C and 4.9 °C for T_i and T_a, respectively, but are greater over the daily time intervals, at 7.6 °C and 10.7 °C respectively. Precipitation events are believed to occur under temperature conditions that differ from the mean daily temperature, leading to large differences in transition range. The uncertainty of the large daily mixed phase transition range needs to be understood to properly inform precipitation phase method selection. As improvements in hydrological modelling necessitate the use of high temporal resolution meteorological observations (Marks *et al.,* 1999) there is little reason to use longer time scales given the much greater scatter in relationship between phase and T_i or T_a at longer intervals.

3.3.2 Model Intercomparison

Quantifying the predictive power of the phase methods, while considering their complexities and data requirements, permits the relative merits of each method to be assessed. The commonly used T0 is simple to use and requires only T_a but provides a very poor approximation of phase. As suggested by Marks *et al.* (2013), replacing the $T_a$threshold with a T_i threshold appreciably increases the accuracy, but also requires humidity measurements. Daily $T_a$methods calibrated from large datasets (UBC) performed well and could outperform the proposed semi-physical psychrometric method on daily time steps where no local calibration was available. Where a local calibration was available, the Kienzle method performed well because of its non-linear functions, but at sites without local calibration its performance was degraded despite it being derived on the eastern slopes of the Canadian Rockies near to MC. The proposed semi-physical psychrometric energy balance model (PSY) was consistently the most robust and accurate at most time steps and sites and shows little loss in performance between calibration and validation sites. At sub-daily time intervals it consistently performed better than any other method. Although the model performance improved as time step length decreased there was little difference between hourly and 15 minute time steps, suggesting that use of hourly data is adequate for phase estimation using the PSY model.

CHAPTER 4. Uncertainty of Phase Methods in Hydrological Process Modelling

This chapter addresses the third objective to quantify the uncertainty that empirical phase methods introduce into cold regions hydrological modelling. The chapter describes the model used, the Cold Regions Hydrological Modeling platform (CRHM), the various sites modelled, the modelling approach, analysis methodology and the results. The discussion focuses on the hydrological response unit (HRU) and basin scale uncertainty relationships, assessment of model performance and limitations.

4.1 Cold Regions Hydrological Model

The Cold Regions Hydrological Modeling platform (CRHM) was used to assess the effect of the uncertainty of precipitation phase models on HRU and basin scale hydrological processes. CRHM is a physically based modular hydrological modeling platform based on decades of coordinated cold region hydrological process research in western and northern Canada (Pomeroy *et al.,* 2007). The model's process representations include blowing snow, snow interception, sublimation, snowmelt, infiltration into frozen soils, hillslope water movement over permafrost, actual evaporation, radiation exchange to complex surfaces, soil moisture balances and streamflow routing. CRHM links hydrologic processes to meteorological observations and basin characteristics and allows a model's complexity to vary, from conceptual to physically-based representations, to match the data availability and uncertainty in the parameters of the basin in question. CRHM uses hydrological response units (HRU) which comprise spatial units of mass and energy balance calculations that are related to biophysical landscape units. The platform is useful for hydrological prediction, diagnosing the adequacy of hydrological understanding and for assessing the uncertainty of hydrological process algorithms.

4.2 Hydrological Models

The effect of precipitation phase uncertainty in hydrological modelling was assessed at HRU and basin scales. HRU scale simulations for four hydrologically distinct HRUs in a CRHM model of MC give insight into how differing hydrological process are affected by precipitation phase uncertainty. Basin scale CRHM models simulated the hydrology of several basins (Figure 4.1)

including MC, Wolf Creek (WC), Granger Basin (GB) and Bad Lake (BL) demonstrating how precipitation phase and hydrological uncertainty varies with climate and basin physiography.

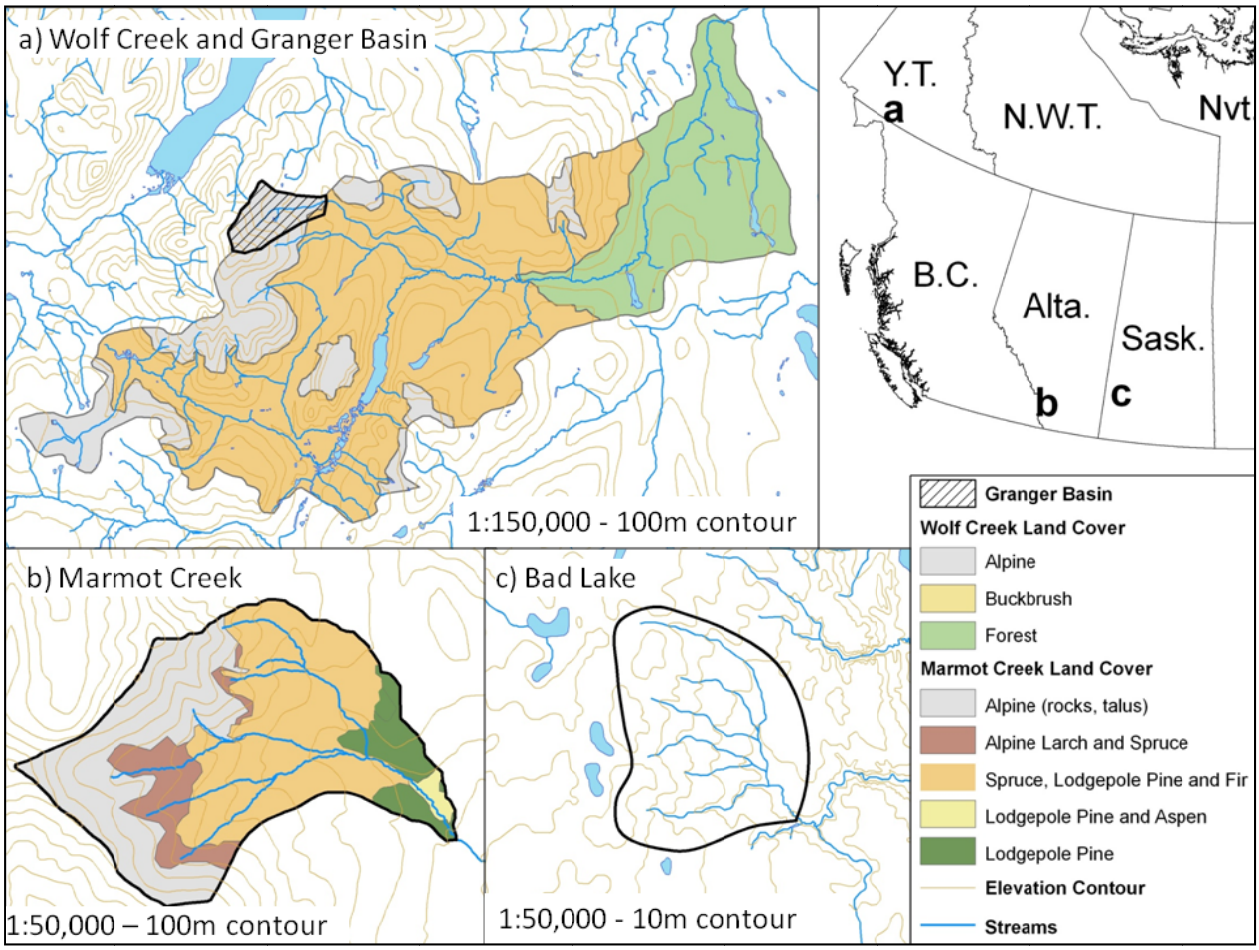

Figure 4.1: Research Basins showing land cover and location in western Canada.

4.2.1 Marmot Creek Research Basin

The schematic diagram of the CRHM model for the Marmot Creek Research Basin (MC) is shown in Figure 4.2. The model structure and parameters used in this study are taken from Fang *et al.* (2013) which contains a full discussion of the model setup and parameter selection. The model uses 36 HRUs divided among four sub-basins to capture the complex hydrological responses in a sub-alpine basin that spans valley bottom forest to exposed alpine domains. The mountain environment hydrological processes that the MC model calculates (and their references) include:

- incoming radiation to slopes (Garnier and Ohmura, 1970)
- longwave radiation (Sicart *et al.,* 2006)

- snow albedo decay (Verseghy, 1991)
- canopy processes including rainfall and snowfall interception, sublimation and sub-canopy radiation (Pomeroy *et al.,* 1998; Ellis *et al.,* 2010)
- blowing snow redistribution and sublimation (Pomeroy and Li, 2000)
- snowmelt from an energy-balance model (SNOBAL) (Marks *et al.,* 1998)
- all-wave radiation for evapotranspiration (Granger and Gray, 1990)
- frozen soil infiltration (Zhao and Gray, 1999) and rainfall infiltration (Ayers, 1959)
- actual evapotranspiration from unsaturated surfaces using an energy balance and extension of Penman's equation to unsaturated conditions (Granger and Gray, 1989; Granger and Pomeroy, 1997) and evaporation from saturated surfaces (Priestley and Taylor, 1972)
- hillslope processes based on a soil moisture balance developed by Leavesley *et al.* (1983) and modified by Dornes *et al*. (2008) and Fang *et al*. (2010) to quantify surface – groundwater interactions and sub-surface flow. The subsurface is divided into recharge and lower soil layers, which interact with surface hydrological processes. These upper layers in turn interact with a saturated groundwater layer. Lateral and vertical flows are calculated between all layers with an implementation of Darcy's law taking into account differences in HRU slope, saturated hydraulic conductivities and pore size distribution (to quantify unsaturated hydraulic conductivities via the Brooks and Corey (1964) relationship)
- water routing among the HRUs and between sub-basins using the Muskingum method (Chow, 1964)

The precipitation phase methods were also evaluated at a HRU scale in MC to calculate the effect that phase uncertainty had on HRUs with differing dominant hydrological processes (as shown in Table 4.1). The HRU models were similar to the basin model except that:

- UC did not include canopy processes or blowing snow redistribution and sublimation as it represents a forested clearing.
- UF did not include blowing snow redistribution and sublimation as it represents a forest.
- RT did not include canopy processes as it represents an exposed alpine ridge.

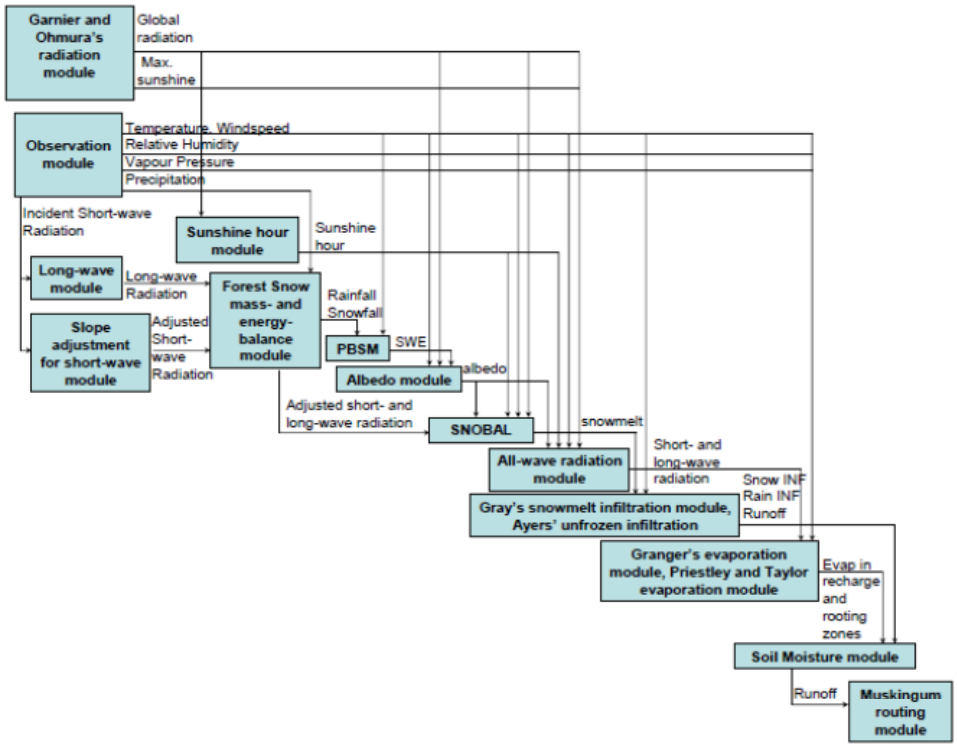

Figure 4.2: Flow chart of physically based hydrological modules for simulating hydrological processes at Marmot Creek (Fang *et al.,* 2013).

Table 4.1: MC HRU Scale Hydrological Response Units

HRU	Abbreviation	Description	Important Hydrological Processes	Snow Course Point Spacing (m)	Number of Snow Course Depth Points
Upper Forest	UF	mid elevation forest (10000 m^2)	interception	5	13-16
Upper Clearing	UC	mid elevation clearing (10000 m^2)	snow accumulation	5	12-21
Fisera Ridge Ridgetop	RT	upper elevation alpine ridgetop (36.9 m^2)	blowing snow (source)	3-5	6-32
Fisera Ridge Forest	FO	upper elevation tree line larch forest (15 m^2)	blowing snow (sink), interception	3-5	4-19

The locations of these sites are shown in Figure 3.1. The soil moisture state variables, for the HRU and basin scale, were reinitialised from observations each model year. The years modelled spanned 2006-2011 for the entire basin and 2008-2011 for the HRU scale. Streamflow and snow survey data were used to evaluate the model performance. Streamflow data (1963-present) was taken from a Water Survey of Canada hydrometric station, which was a v-notch weir, at the mouth of the Marmot Basin. The snow courses consist of fixed transects with observation of snow depths (ruler) and densities (typically taken using ESC-30 snow tubes). The spacing and number of points varies considerably among survey sites and are summarized in Table 4.1. A density measurement was typically taken every three points but this varied by snow survey.

4.2.2 Wolf Creek

The Wolf Creek Research Basin (WC) is located in the Upper Yukon River Basin near Whitehorse, Yukon. The headwater basin, in the northern Coast Mountains, ultimately contributes to the regionally significant Mackenzie River system. The basin area is ~195 km^2 and spans alpine tundra, subalpine taiga and boreal forest ecosystems. The climate is cold and dry. Climate normals (1971-2000) reported from the Whitehorse International Airport (WIA), located 15 km north of WC, show the daily annual mean T_a value is 0.7 °C with the coldest (January) and warmest months (July) having daily mean T_a values of -17.7 °C and +14.1 °C respectively (MacDonald *et al.,* 2009). The annual precipitation is between 300 and 400 mm, of which approximately 40% is snowfall (Pomeroy and Granger, 1999). Hydrometeorological observations, by a consortium of researchers from Yukon Environment, Environment Canada and the University of Saskatchewan amongst others, began in 1993 in order to develop hydrological models suitable for the region (Pomeroy *et al.,* 2010). Observations available for this analysis spanned 1994 to 2002. Pomeroy *et al.* (2010) give a complete discussion of WC model setup and parameter selection. The WC model is much simpler than the MC model as there is larger parameter uncertainty due to less information on the spatial distribution of hydrologically relevant biophysical factors, a smaller number of observation sites and the larger basin area negating the advantages of more HRUs and complexity. The hydrological processes that the WC model calculates are similar to the MC model with the only differences being:

- incoming shortwave radiation is estimated with a semi-empirical approximation (Annandale *et al.,* 2004, Shook and Pomeroy, 2011)

- snowmelt calculated with the Energy-Budget Snowmelt Model (Gray and Landine, 1988)
- snow albedo calculated with method from Gray and Landine (1987)
- soil routine modified by Dornes *et al.* (2008) for tundra soils
- all routing quantified with Clark's lag and route algorithm (Clark, 1945)

Only three HRUs are utilized (Alpine, Tundra and Shrub) which correspond to the ecosystem units determined by Janowicz (1999).

4.2.3 Granger Basin

Granger Basin (GB), a small (8 km^2) alpine sub-basin of WC, was also modelled. The GB model was developed to study snow processes, redistribution and melt, in subarctic environments (Dornes *et al*., 2008; MacDonald *et al.,* 2009). The model uses five HRUs which comprise the upper basin, plateau, valley bottom, north and south facing slopes. As well as the differences in HRUs and basin size, the GB model differs from the WC model in that it does not include the CRHM canopy module due to the lack of forest cover in GB. A complete discussion of model setup and parameter selection is given by Dornes *et al*. (2008), MacDonald *et al*. (2009) and Pomeroy *et al.* (2010). Modeled water years spanned 1999-2001.

4.2.4 Bad Lake

Bad Lake (BL) is an internally drained basin near Totnes in southwestern Saskatchewan. The Creighton tributary of the basin (11.4 km^2) was the site of an International Hydrological Decade research basin that had observations from the 1960s to 1980s (Figure 1). The Creighton tributary basin is dominated by silty clay and clay loam soils with ~85% of the basin area consisting of cultivated agricultural land with the remainder being grassland (Gray *et al.,* 1985). The modeled Creighton tributary is characterized by poorly drained level open land and highland with rolling topography. The tributary is drained by a grassland 'coulee', a sharply incised valley in the upland plain. Like most prairie streams it flows intermittently with the majority of discharge associated with the snowmelt period. The basin is semi-arid with ~300 mm of annual precipitation (Gray and Granger, 1986). The BL model quantified the following hydrological processes for a prairie environment:

- incoming radiation to slopes (Garnier and Ohmura, 1970)
- snow albedo calculated from method from Gray and Landine (1987)
- blowing snow redistribution and sublimation (Pomeroy and Li, 2000)

- snowmelt calculated with the Energy-Budget Snowmelt Model (Gray and Landine, 1988)
- snowmelt frozen soil infiltration (Zhao and Gray, 1999) and rainfall infiltration (Ayers, 1959)
- actual evapotranspiration from unsaturated surfaces using an energy balance and extension of Penman's equation to unsaturated conditions (Granger and Gray, 1989; Granger and Pomeroy, 1997)
- soil moisture balance based on Leavesley *et al.* (1983) which calculates the soil moisture balance, groundwater storage, subsurface and groundwater discharge, depressional storage, and runoff for control volumes of two soil layers, and a groundwater layer
- surface water routed with the Clark's lag and route algorithm (Clark, 1945)

For a complete discussion of model setup and parameter selection readers are directed to Pomeroy *et al.* (2007). Modeling spanned the 1974 and 1975 water years.

4.3 Methodology

4.3.1 Precipitation Phase Determination in CRHM

Selected precipitation phase methods were implemented in CRHM to understand their differences and uncertainty when used in hydrological process estimation. The standard CRHM model structure uses a double threshold approach whereby a lower temperature (tmax_allsnow) defines all precipitation as snowfall and an upper temperature (tmax_allrain) defines all precipitation as rainfall, with linear interpolation between the two defining mixed phase. A single threshold can be defined with this structure when the tmax_allsnow and the tmax_allrain parameters are the same. Phase methods that do not fit this structure can be implemented rapidly using the macro feature in CRHM. The phase methods implemented in the CRHM models were the single threshold air temperature (T0), the UBC double threshold and the proposed psychrometric energy balance model (PSY). All methods were implemented through manipulation of the tmax_allsnow and the tmax_allrain parameters with the exception of PSY which was implemented through the macro feature (see Appendix A for the macro). These methods are plotted in Figure 4.3a as rain ratio versus T_a; as PSY is a psychrometric function the figure includes PSY rain ratio for several values of relative humidity.

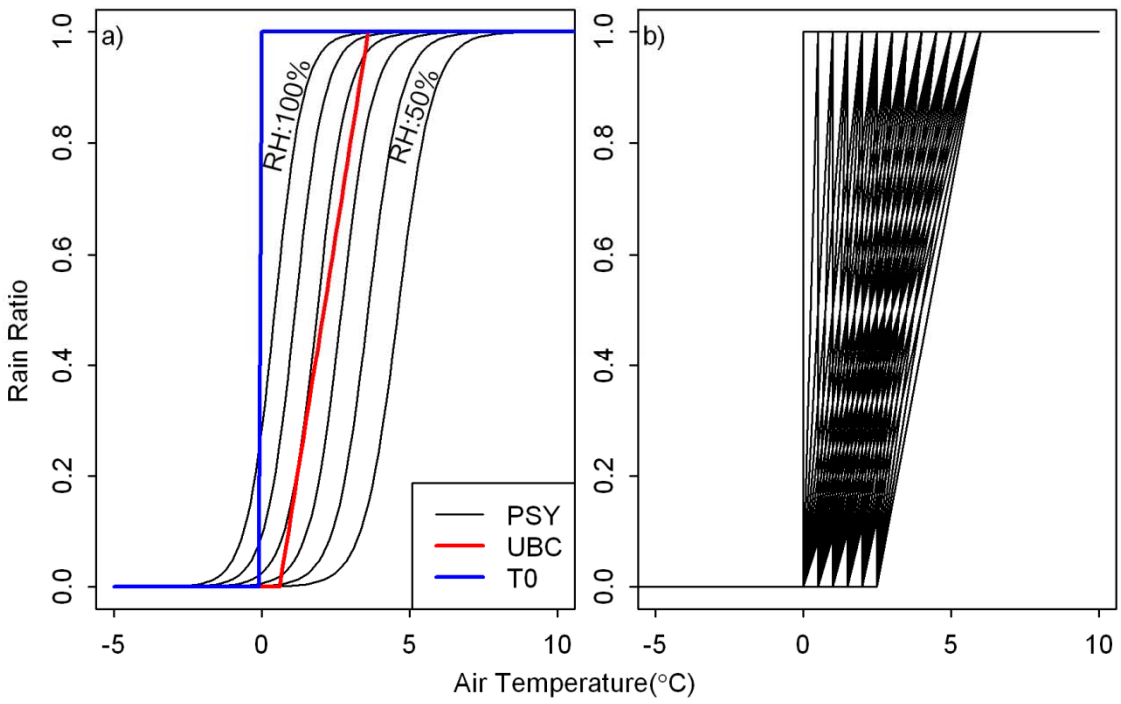

Figure 4.3: (a) Specific precipitation phase methods implemented in CRHM and (b) range of air temperature (T_a) methods to evaluate uncertainty (all permutations of tmax_allsnow (0 °C to 2.5 °C) and tmax_allrain (0 °C to 6 °C) parameters for every 0.5 °C interval) plotted as rain ratio versus air temperature.

4.3.2 Uncertainty analysis

To quantify the uncertainty of T_a based models all permutations of tmax_allsnow (0 °C to 2.5 °C) and tmax_allrain (0 °C to 6 °C) parameters for every 0.5 °C interval, for a total of 63 combinations, were used to run CRHM, as shown in Figure 4.3b. This range in parameters corresponds to the transition range reported by Auer (1974) and many commonly implemented precipitation phase partitioning methods (Wen *et al.,* 2013). The uncertainty of the hydrological processes as a result of varying the T_a methods, hereafter uncertainty, is calculated as follows:

$$uncertainity = \frac{\sum_{i=1}^{n}(Max_i - Min_i)}{n} \quad (4.1)$$

Where Min and Max refers to the lowest and highest values of a model output variable for each time step from the 63 model runs, i is the index (timestep) of the value and n is the number of values (timesteps). The units of each uncertainty are the same as for the hydrologic variable. The hydrologic variables considered are summarized in Table 4.2. The total and peak volumetric

discharge vary with basin size and climate and therefore the uncertainty for discharge was normalized by the basin area expressing volumetric discharge (and volumetric peak) as discharge with units of depth (mm). The uncertainty and differences between specific methods are summarized as mean water year (October 1 to September 30) values.

Table 4.2: Hydrologic Variables Considered

Variable	Units	Description
Rain Ratio	%	Rainfall percentage of precipitation
Daily Runoff	mm	Cumulative daily runoff *
Daily Discharge	mm	Daily discharge (basin discharge as depth = discharge/basin area)**
Peak Discharge	mm	Greatest observed water year daily discharge**
Peak Discharge Day	Days	Date of greatest observed water year daily discharge**
Peak SWE	mm	Maximum annual value of SWE
Snow Free Date	Days	First day in spring when SWE reaches zero (even if subsequent snow accumulation takes place)
Snow Cover Duration	Days	Number of days each water year in with snow on ground, including days of intermittent snowcover in summer

*HRU scale only. Runoff quantifies HRU outflows, **Basin scale only. Discharge quantifies all HRU outflows at basin outlet.

There is a large body of literature on parameter uncertainty in hydrological models (Beck 1987; Melching 1995; Tung 1996; Mcintyre *et al.,* 2002). Common uncertainty estimation techniques include the computationally intensive Monte Carlo methods and generalised likelihood uncertainty estimation (GLUE) (Mcintyre *et al.,* 2002). These methods are effective in quantifying the range of values a suite of parameters can have that can lead to adequate representation of hydrological processes in a calibrated model. The physical basis of CRHM means that the model is not calibrated. All parameters, other than the precipitation phase parameters, did not change throughout the modelling exercise. Monte Carlo and GLUE methods are inappropriate to analyse the uncertainty introduced by T_a phase methods as the range of possible T_a thresholds is known from observation, and does not need to be estimated, and the

variation in hydrological processes is what is of interest. A Monte Carlo approach that randomly samples a parameter distribution has the potential to be useful in this uncertainty analysis. But, as the range in parameters values can be limited by observations, and the range of model output for this parameter space is of interest, the complexities of a Monte Carlo approach are not beneficial and a simple approach that regularly samples the parameter space, as discussed previously, is justified.

4.3.3 Performance Evaluation

To assess the performance of a variety of precipitation phase methods, the model outputs were compared to observations. The MC site dataset was used to assess performance as it has an extensive dataset of reliable streamflow and snow survey observations. The model performance was assessed by quantifying the ability of the model to simulate SWE at the HRU scale and discharge at the basin scale at MC. The model's performance was assessed with the described RMSD and MB.

4.4 Results

4.4.1 Uncertainty at HRU Scales

The effects of phase methods at a HRU scale were assessed using selected HRUs in MC. The uncertainties of the methods are summarised in Tables 4.3 and 4.4 respectively. The largest consequence of varying the phase methods is to change the rain ratio (Figure 4.4). At a HRU scale, the uncertainty can be large with the greatest uncertainty occurring during the summer months. During winter months less uncertainty is estimated at UF and UC with even less uncertainty estimated at RT and FO. Over the modeling period, uncertainty was slightly greater at UF and UC (representing 18.5% and 20.2% of their respective rain ratios) than RT and FO (17.9% and 17.2% of their rain ratios). The UBC and PSY models (Table 4.4) have smaller rain ratios than T0 with the differences greater in summer months and less during winter months at UF and UC and nearly identical at RT and FO. Slight differences between UBC and PSY are evident with PSY rain ratios being slightly greater for summer months and smaller for shoulder (fall and spring) and winter months.

Table 4.3: Uncertainty of air temperature methods in hydrological process simulations.

Variable	Units	Uncertainty			
HRUs		UC	UF	RT	FO
Rain Ratio	%	**20.2**	18.5	17.2	17.9
Daily Runoff	mm	0.47	0.21	0.58	**1.48**
Peak SWE	mm	43.9	18.6	63.8	**159.6**
Snow Free Date	Days	**25.5**	20.2	15.5	20.8
Snow Cover duration	Days	**35.8**	30.5	28.2	35.2
Basins		MC	GB	WC	BL
Rain Ratio	%	18.3	**18.6**	16.4	10.5
Daily Discharge	mm	**0.40**	0.12	0.03	0.15
Peak Discharge	mm	4.6	**6.6**	1.0	2.2
Peak Discharge Date	Days	7	**10.0**	5.9	0.0
Peak SWE	mm	**35.4**	7.4	4.2	2.0
Snow Free Date	Days	**16.2**	5.7	11.4	-2.0
Snow Cover duration	Days	24.8	16.3	**35.2**	3.0

Note: values correspond to the mean water year uncertainty and bold values represent the greatest uncertainty.

The uncertainty in the daily runoff, as plotted by Figure 4.5, varies directly with the amount of runoff, as both greatest in spring and summer months. The uncertainty range for annual runoff over the modeling period is quite large, as is shown in Table 4.3. The UBC and PSY models give similar results and generally estimate more runoff than T0, although UBC simulated runoff events during the summer months at UC and UF that PSY and T0 do not.

The uncertainty in daily SWE increases over the course of the winter season and peaks during the spring snowmelt, and is shown in Figure 4.6. The uncertainty in the peak SWE can vary by up to 160 mm (Table 4.3). The annual snow free date and snowcover duration can vary significantly by up to 26 and 36 days respectively at UC. The T0 method coincides with the lower bound of the uncertainty, and PSY model consistently simulates higher SWEs with a later and higher peak SWE and a later snow free day. UBC simulates a slightly higher later peak SWE than T0.

Table 4.4: Method comparison of phase methods in hydrological process simulations.

Variable	Units	UBC				T0			
HRUs		UC	UF	RT	FO	UC	UF	RT	FO
Rain Ratio	%	-2.3	-3.8	-2.7	-2.9	7.7	5.9	6.8	7.0
Daily Runoff	mm	0.003	0.02	0.04	0.01	-0.08	-0.03	-0.06	-0.11
Peak SWE	mm	-42.3	-21.4	-41.7	-67.7	-59.7	-31.3	-71.3	-127
Snow Free Date	Days	-14.8	-10.2	-6.8	-9.0	-28.5	-21.2	-15.5	-20.5
Snow Cover duration	Days	-6.0	-2.2	0.2	-10.2	-25.8	-17.5	-16.2	-27.8
Basins		MC	GB	WC	BL	MC	GB	WC	BL
Rain Ratio	%	-3.4	-5.1	-2.0	-1.40	5.9	5.5	5.7	2.7
Daily Discharge	mm	-0.05	-0.04	-0.003	0.04	0.03	0.03	0.003	-0.01
Peak Discharge	mm	-0.6	-3.0	-0.2	-0.2	0.4	2.7	-0.2	-1.2
Peak Discharge Date	Days	1.3	4.70	-0.2	0.0	-2.3	-5.3	-4.4	-0.5
Peak SWE	mm	-17.4	0.0	0.4	0.2	-31.7	-4.6	-2.5	-1.0
Snow Free Date	Days	-4.2	2.0	-1.4	-1.0	-14.0	-3.0	-8.1	0.5
Snow Cover duration	Days	0.2	3.3	-11.2	0.0	-14.0	-5.3	-33.2	-1.5

Note: UBC and T0 values presented as absolute difference from PSY

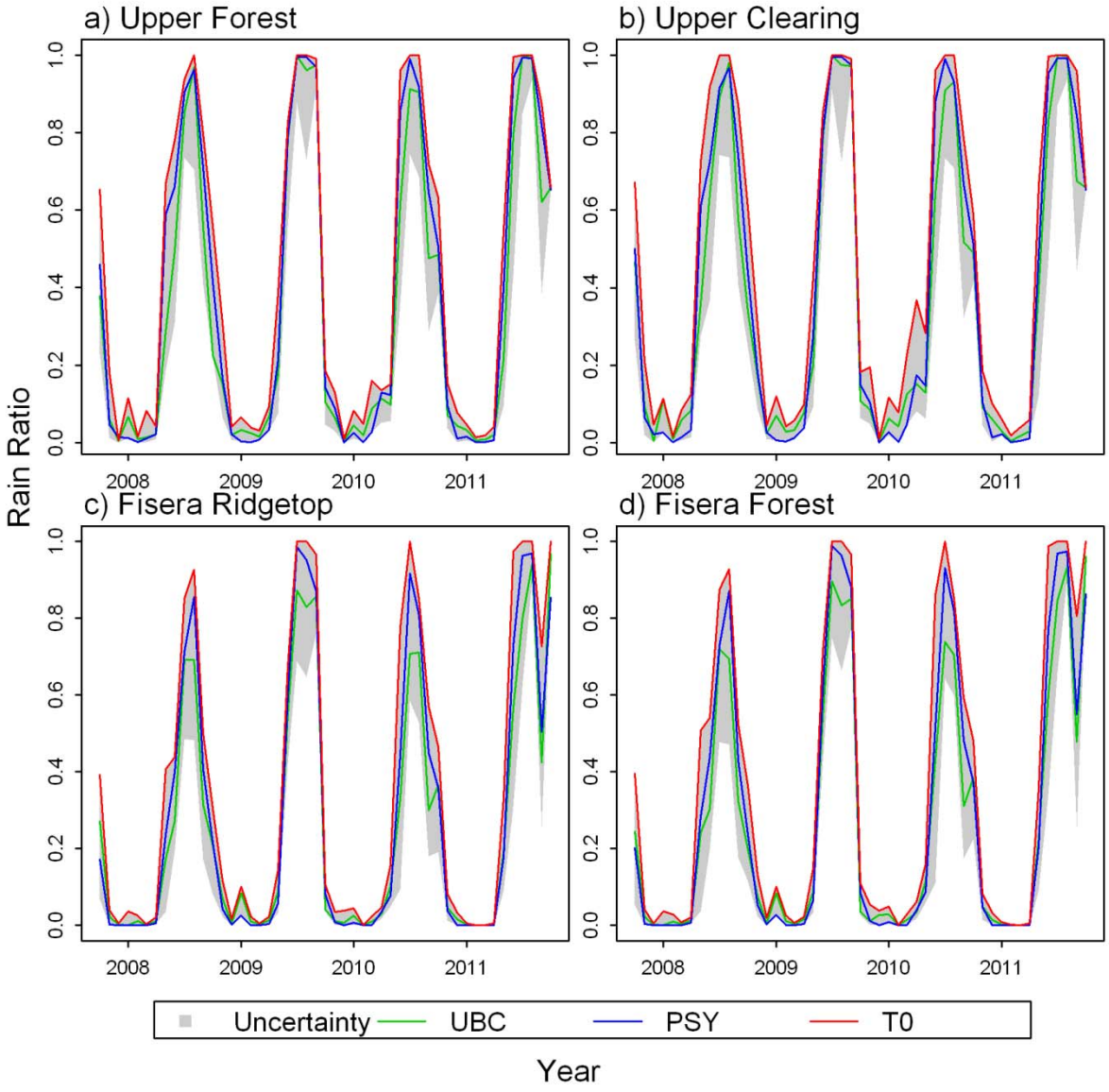

Figure 4.4: Monthly rain ratio for (a) Upper Forest (1848 m), (b) Upper Clearing (1845 m), (c) Fisera Ridgetop (2323 m), and (d) Fisera Forest (2294 m). Uncertainty is plotted as grey area overlain by UBC (green), PSY (blue) and T0 (red) lines.

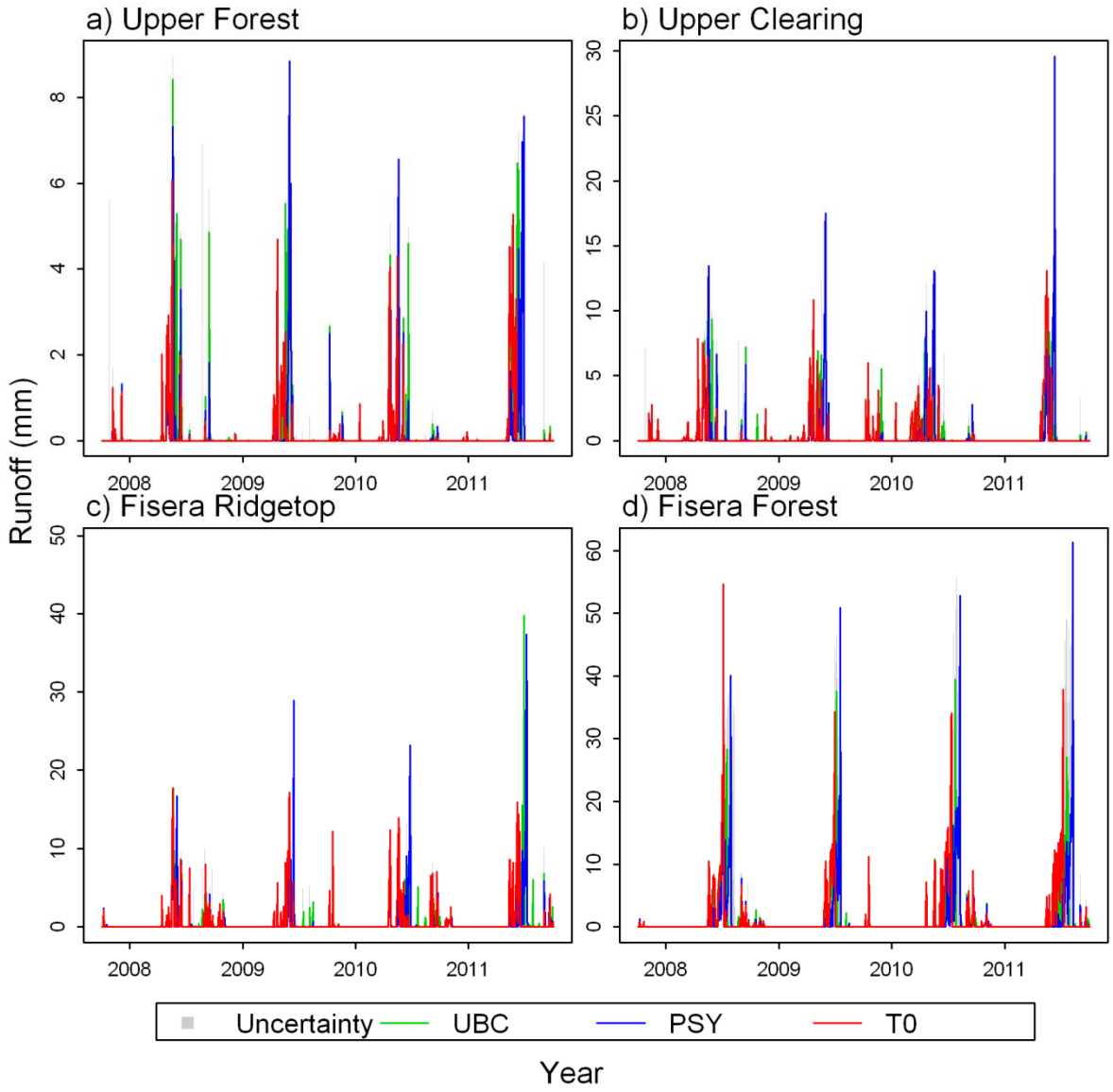

Figure 4.5: Daily runoff for (a) Upper Forest (1848 m), (b) Upper Clearing (1845 m), (c) Fisera Ridgetop (2323 m), and (d) Fisera Forest (2294 m). Uncertainty is plotted as grey area overlain by UBC (green), PSY (blue) and T0 (red) methods.

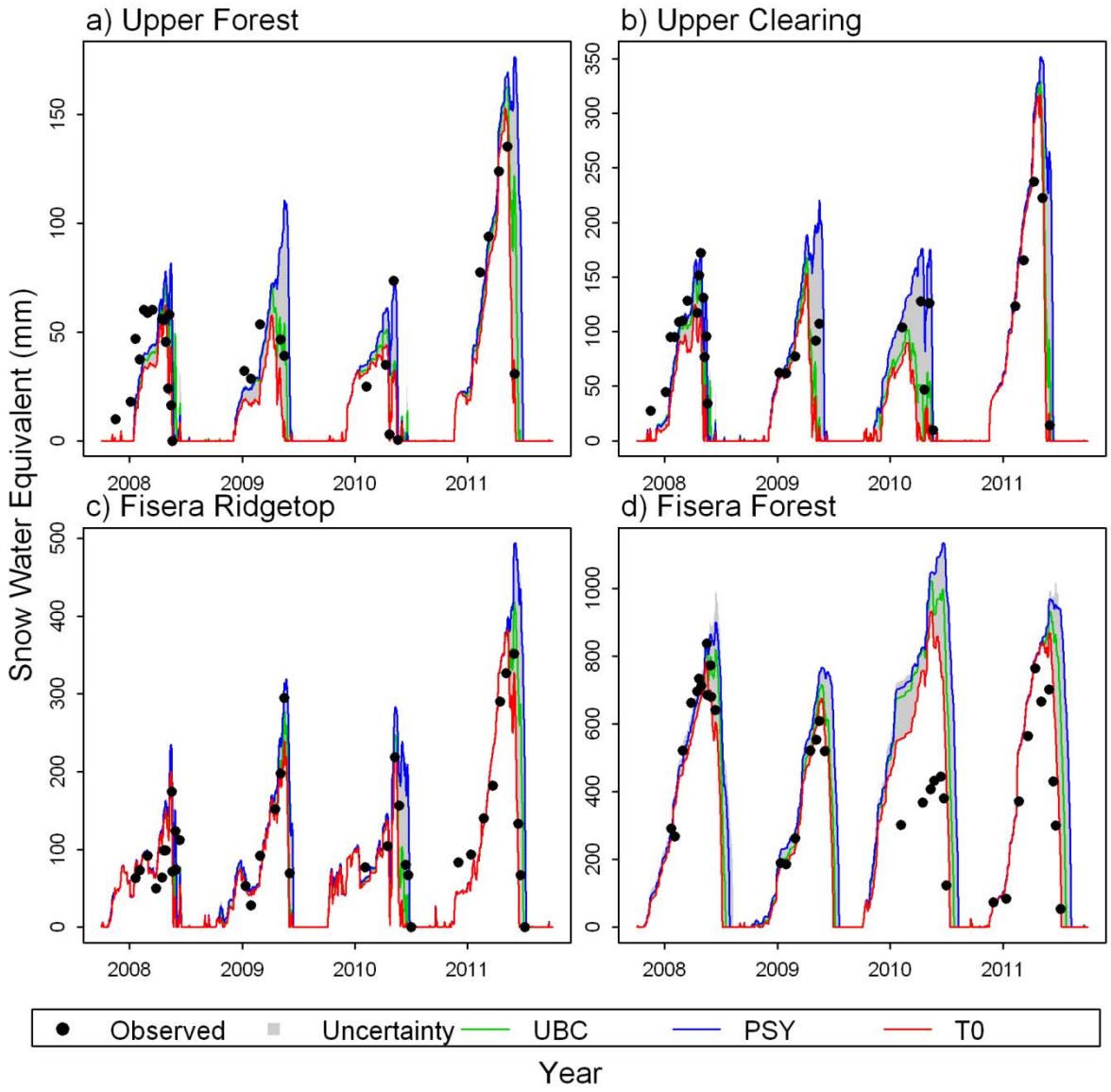

Figure 4.6: Daily SWE for (a) Upper Forest (1848 m), (b) Upper Clearing (1845 m), (c) Fisera Ridgetop (2323 m), and (d) Fisera Forest (2294 m). Uncertainty is plotted as grey area overlain by UBC (green), PSY (blue) and T0 (red) methods. Observed SWE is plotted as black dots.

4.4.2 HRU Scale Performance

Simulations of SWE over the four HRUs in question show large uncertainty that directly affects the performance of SWE simulations. The uncertainty is greater in some years than others (Figure 4.6b). Figure 4.6b shows little uncertainty in 2009, but much greater uncertainty in 2010. This difference is believed to be due to more precipitation events occurring near the phase transition thresholds increasing the uncertainty in rain ratio, Figure 4.4b and in turn snow

accumulation, Figure 4.6b. The statistical performance of a select group of methods is presented in Figure 4.7. Statistical performance varies among the HRUs with the smallest MB at UF and RT followed by UC and FO. The RMSD is similar to MB with best performances at UF followed by UC and RT, which are very similar, with a large increase in error at FO. The FO RMSD and MB values show that the performance for the FO HRU model is degraded relative to other HRUs. The relative performance of the methods with respect to one another at these HRUs shows some patterns. Generally UBC (T0) showed better performance at UC (FO). Method performance was less clear at UF and RT where T0 produced smaller RMSD while UBC produced smaller MB. PSY, which overestimates snow accumulation, consistently shows the poorest statistical performance.

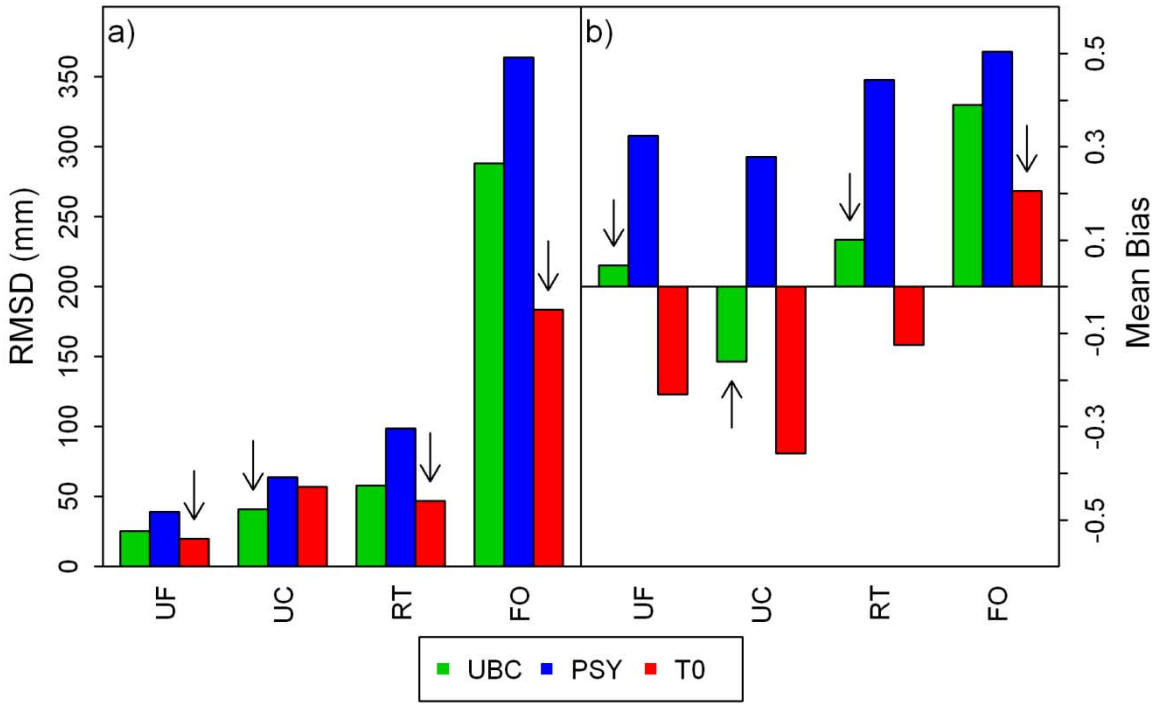

Figure 4.7: (a) Root mean square error (RMSD) and (b) mean bias (MB) of UBC (green), PSY (blue) and T0 (red) methods to simulate SWE on the HRU scale at various HRUs including Upper Forest (UF), Upper Clearing (UC), Fisera Ridge: Ridgetop (RT), and Fisera Ridge: Forest (FO). The arrows show the methods having best performance for each test and HRU.

4.4.3 Uncertainty at Basin Scales

The effects of differing phase methods on basin scale models were assessed at MC, WC, GB and BL. The uncertainty for the T_a models is summarised in Table 4.3 and the differences among

methods are summarised in Table 4.4. As in the HRU tests, the phase method used has a large effect on the rain ratio, weighted by area, at the basin scale as shown in Figure 4.8. The uncertainty varies seasonally, showing the greatest uncertainty over the summer months for the MC, GB and WC models. The BL model is different from the others as it has the greatest uncertainty in rain ratio during the shoulder months due to the extreme climate. The WC and GB models show reduced rain ratio uncertainty in the winter months. The uncertainty due to the T_a methods across the modeling period showed the rain ratio varied the most in the MC model and least in the BL model. UBC and PSY consistently estimated a smaller rain ratio than did T0. The differences among the models were greater in summer months for the MC, GB and WC models while differences were minimal during winters in the GB, WC and BL models. In the MC model the PSY estimated a smaller rain ratio than did UBC during the winter months.

The uncertainty in the daily basin discharge, as shown in Figure 4.9, is similar to the runoff patterns observed on the HRU scale in that it is related to the magnitude of modelled discharge; both the discharges and uncertainties are greatest in spring and summer months. The uncertainty in the discharge over the modeling period is smaller in magnitude than that associated with HRU scale runoff and is greatest in the MC model. The T0 tends to estimate more discharge, while UBC tends to estimate less than PSY. The BL model is opposite with T0 simulating less discharge (-0.01 mm) and UBC simulating more discharge (0.04 mm) relative to PSY. The uncertainty in absolute peak discharge is greatest in the GB model. Compared to PSY, UBC estimates a lower annual peak and T0 tends to estimate a larger value for the annual peak with the exception of the WC and BL models which show peaks -0.2 and 1.2 mm less than PSY. The uncertainty of the annual timing of the discharge peak varies the most, by 10 days in the GB model. The T0 method simulates an earlier annual peak relative to PSY. The UBC method shows variability with respect to PSY in that annual peak occurs 1.3 and 4.7 days after for the MC and GB models with minimal difference for the WC model. The BL model shows very little uncertainty in terms of annual peak timing.

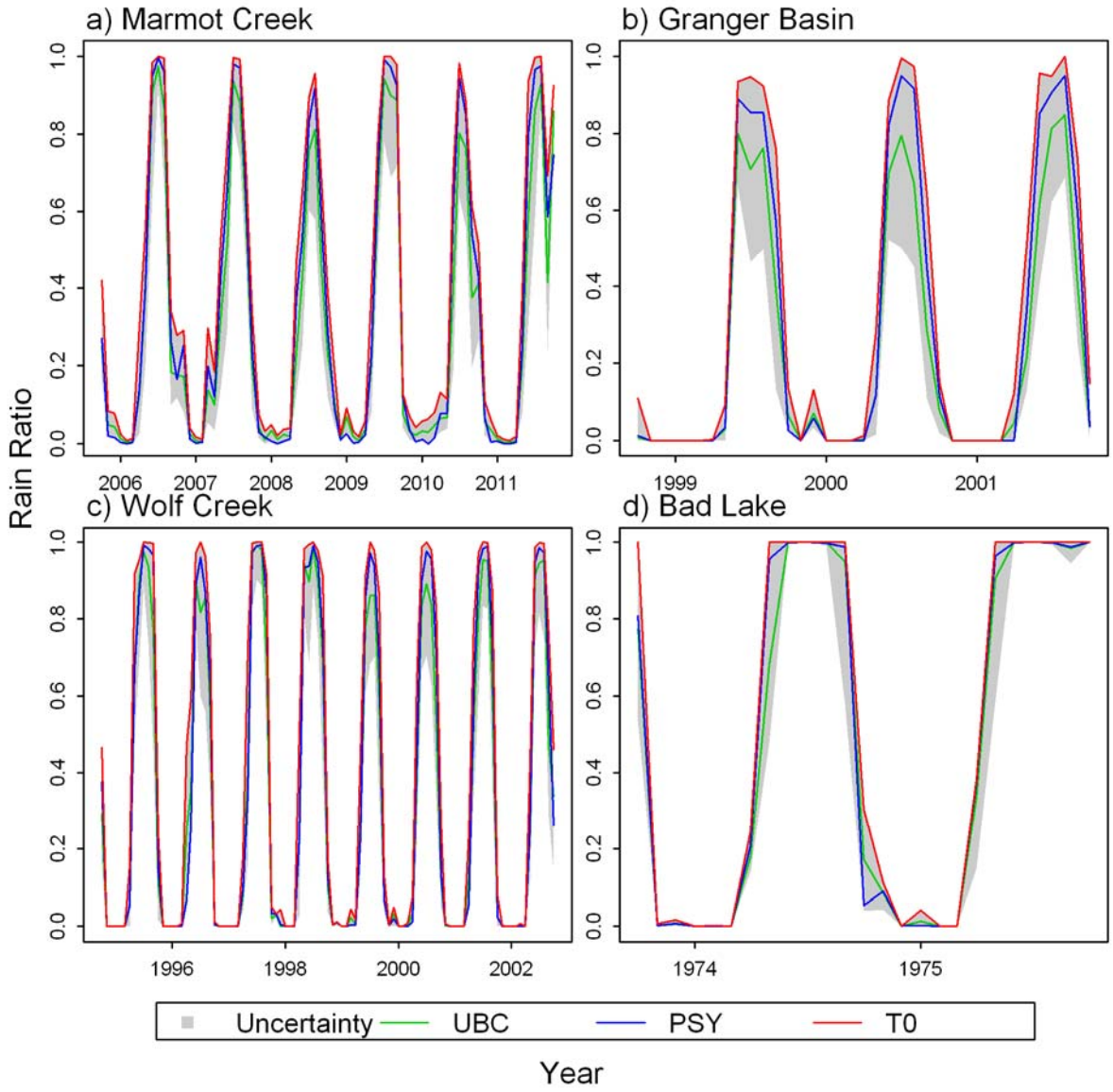

Figure 4.8: Monthly rain ratio for (a) Marmot Creek, (b) Granger Basin, (c) Wolf Creek, and (d) Bad Lake. Uncertainty is plotted as grey area overlain by UBC (green), PSY (blue) and T0 (red) methods.

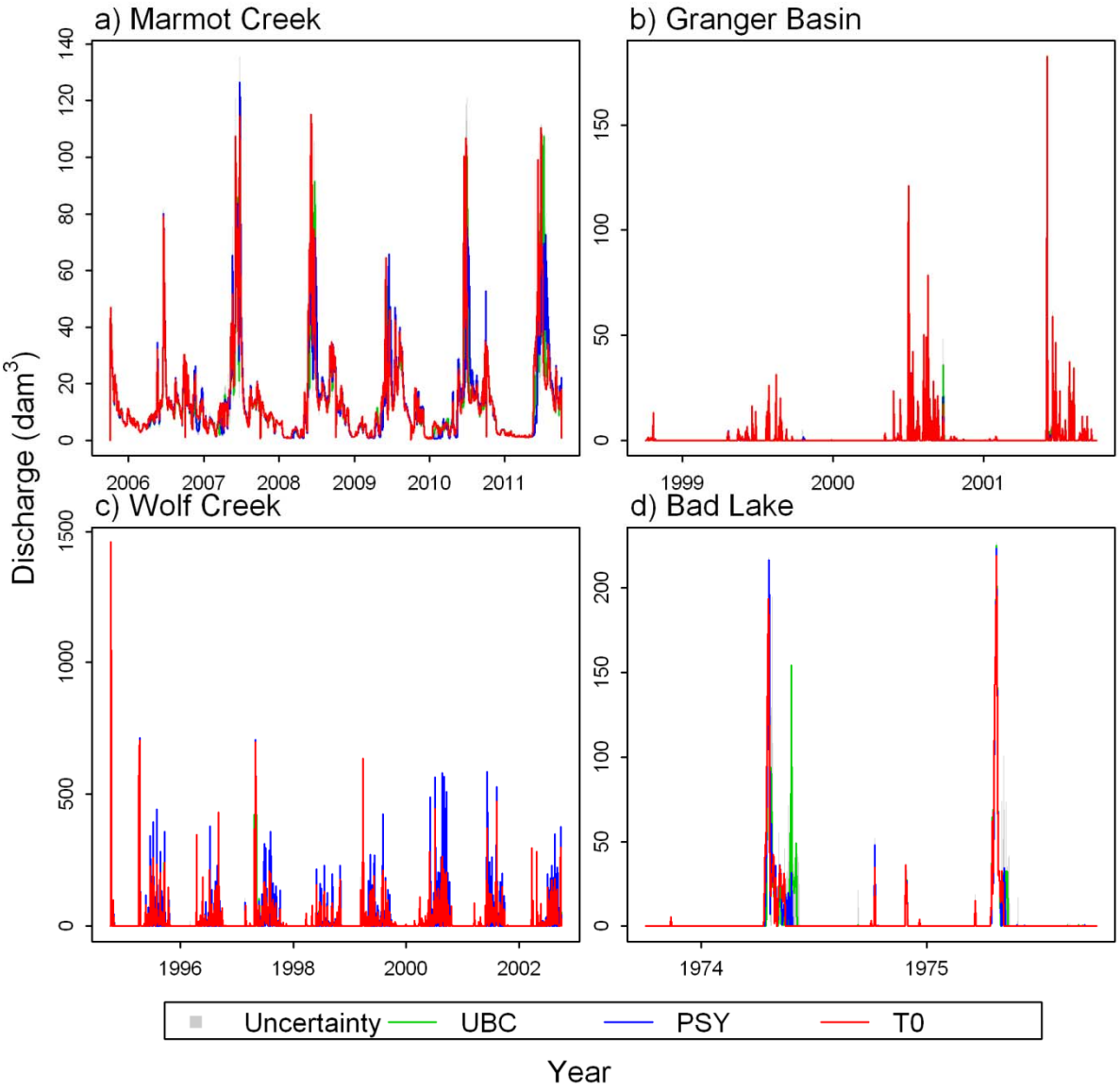

Figure 4.9: Daily discharge for (a) Marmot Creek, (b) Granger Basin, (c) Wolf Creek, and (d) Bad Lake. Uncertainty is plotted as grey area overlain by UBC (green), PSY (blue) and T0 (red) methods.

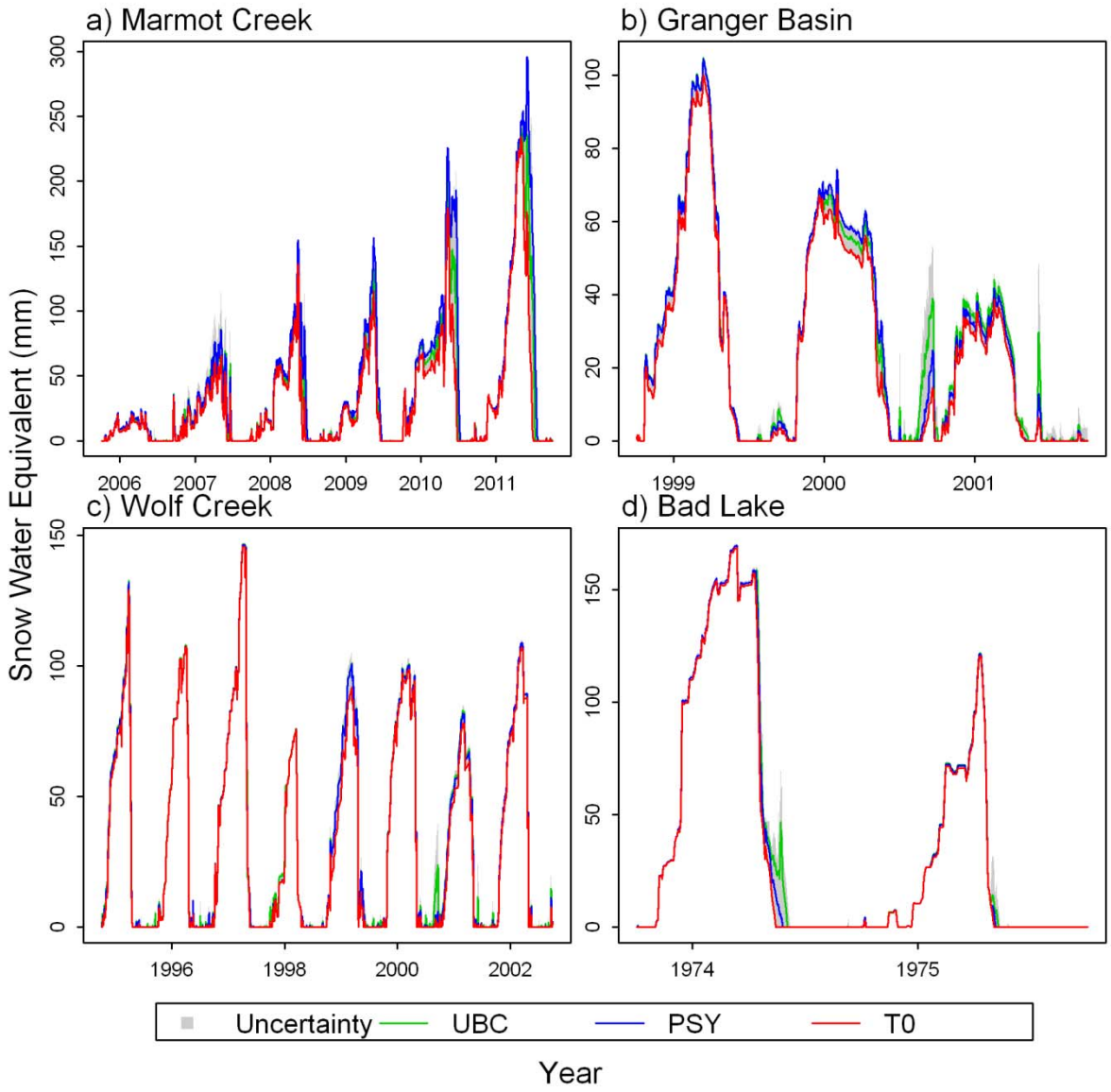

Figure 4.10: Daily SWE for (a) Marmot Creek, (b) Granger Basin, (c) Wolf Creek, and (d) Bad Lake. Uncertainty is plotted as grey area overlain by UBC (green), PSY (blue) and T0 (red) methods.

Over the modeling period, the uncertainty of daily SWE, Figure 4.10, varied the most in the MC model. This observation is confirmed by the uncertainty of the peak SWE being greatest in the MC model with a value of 35.4 mm. As seen at the HRU scale, the T0 method coincides with the lower bound of the uncertainty. On average, UBC estimates less peak SWE in the MC model relative to PSY (-17.4 mm), in contrast to simulating very similar SWE at the GB, WC and BL models. Seasonally there is complexity in the UBC-PSY relationship as during the GB winters

PSY simulates greater, and in shoulder and summer seasons, less SWE. The annual snow free day and snowcover duration uncertainties also vary between basins. The uncertainty shows that annual snow free day varies the most (least) in the MC (BL) models. Both UBC and T0 annual snow free day tends to occur earlier than PSY. The uncertainty associated with the duration of annual snowcover on average varies by up to 36 days in the WC model. The T0 simulates annual snowcover duration that is shorter than those simulated by PSY, up to 33 days in the WC model. In contrast, UBC does not vary from PSY for the MC and BL models while duration is simulated to be 3 days longer for the GB model and 11 days shorter for the WC model.

4.4.4 Basin Scale Performance

To assess the basin scale performance of the precipitation phase methods, the MC basin discharge was simulated and compared to observations (Figure 4.11). Although continuous simulations were generated for MC, streamflow is only observed from May to October by a Water Survey of Canada gauge, so the statistical comparison was restricted to the open water season as plotted in Figure 4.11. Figure 4.12 shows that all methods overestimate discharge (RMSD and MB) as the CRHM model tends to overestimate the late season recession limb of the annual hydrograph. The best performance is found with the UBC method.

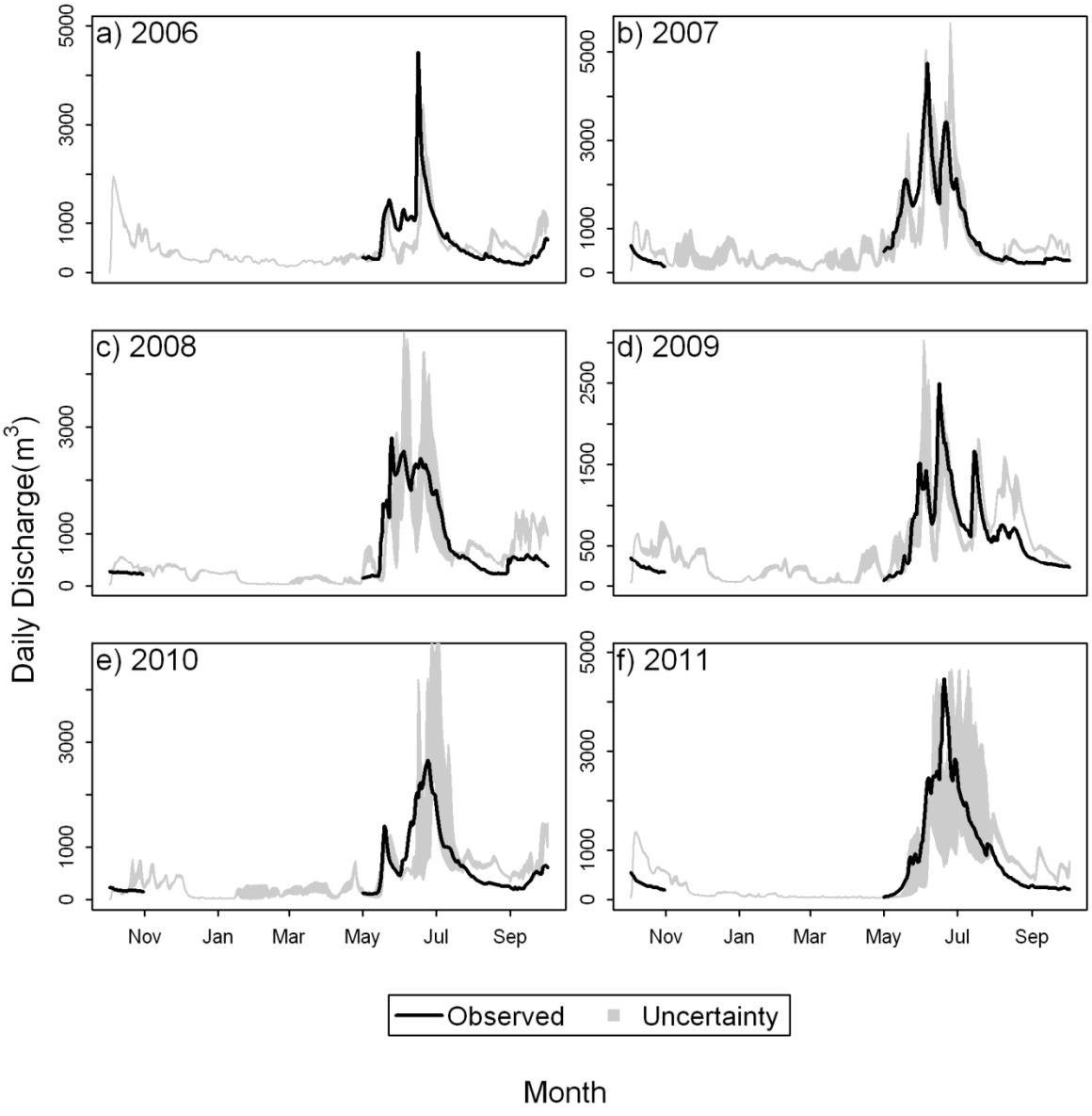

Figure 4.11: Marmot Creek observed discharge (black line) relative to modeled uncertainty for water years 2006 through 2011.

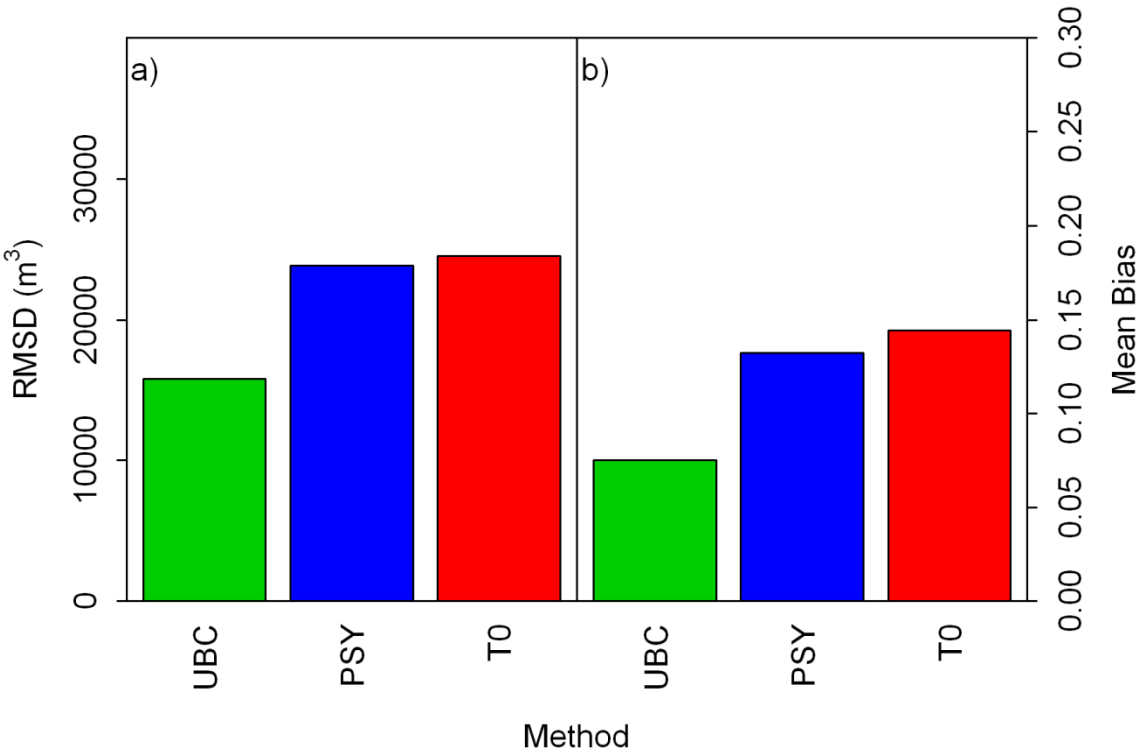

Figure 4.12: (a) Root mean square error (RMSD) and (b) mean bias (MB) of UBC (green), PSY (blue) and T0 (red) methods to simulate seasonal discharge on the basin scale over Marmot Creek.

4.5 Discussion

Varying the phase methods in a hydrological model changes the estimated quantities of rainfall, snowfall and total precipitation. The phase methods affect the timing of rainfall and snowfall, complicating the understanding of a hydrologic response to varying phase. The hydrological response to these changes varies considerably by basin and by variable.

As discussed in Chapter 3, the PSY and T0 models tend to estimate more rainfall (and less snowfall) than double threshold models like UBC. The UBC identifies more precipitation as snowfall than T0, which identifies as rainfall all precipitation above 0 °C. The UBC and T0 methods disregard the atmospheric humidity during precipitation and are difficult to directly relate to the PSY model, which includes *RH*. Generally PSY identifies more precipitation as rainfall than T0. In addition the smaller transition range from snowfall to rainfall for PSY begins and ends at lower T_a than UBC resulting in less precipitation being identified as snowfall with PSY (Figure 4.3a).

The identification of phase affects the amount of precipitation modeled, due to wind-induced undercatch, which is a consequence of the deformation of the wind field over a gauge orifice, causing displacement and acceleration of snow particles and reduced effective fall velocities (Thériault *et al.,* 2012). Undercatch is often corrected for in hydrological modeling and varies with the amount of snowfall identified. The uncertainty of undercatch due to differing phase methods varies by basin as it is influenced by the wind speeds and the fraction of precipitation occurring near the transition range. Due to data limitations at Wolf Creek and Granger Basin, wind-induced undercatch was corrected by direct correlation to a corrected precipitation record at WIA prior to the CRHM runs. Only the Marmot Creek and Bad Lake CRHM models handled the undercatch correction, Marmot Creek with a method from MacDonald and Pomeroy (2007) and Bad Lake with a method from Goodison (1978), resulting in annual total precipitation differing by 20 mm and 12 mm between the UBC and T0 models for the basins respectively.

4.5.1 HRU scale Relationships

The influence of elevation on phase separation is apparent in Figure 4.4. As T_a generally decreases with elevation, due to adiabatic expansion, the warmer winter air temperatures at lower elevations are nearer the transition range leading to greater rain ratio uncertainty. Upper elevations sites show almost no uncertainty in winter as conditions are much colder than the phase thresholds.

The high uncertainty of simulated runoff is largely due to how phase identification affects short-term differences in runoff generation processes. Uncertainty in hydrological processes is determined by calculating the daily maximum and minimum output values from the range in T_a models for the variable of interest. As a result the timing of runoff can have a large role in increasing the uncertainty of runoff. If one model shows runoff occurring a day later than another then the runoff uncertainty for those two days will have a minimum value of 0 and a large maximum value on both days. The total runoff is closely associated with amount of snowmelt at MC which in turn can be related to the amount of snow accumulation and specific processes at work. The FO model, which simulates a treeline drift, shows the largest uncertainty, as blowing snow deposition is very sensitive to precipitation phase. RT (blowing snow source), UC (no interception) and UF (interception) show less runoff uncertainty. Hydrological processes which

remove mass (interception and blowing snow for source HRUs) lead to a reduction in uncertainty while processes that add mass (such as blowing snow for sink HRUs) are more sensitive to phase methods.

The uncertainties depicted in Table 4.3 of peak SWE, snow free date and snowcover duration, demonstrate that RT and FO have the greatest uncertainty while UC and UF have the smallest uncertainty. This difference in uncertainty among the sites is due to the same processes affecting the runoff uncertainty described previously. The snow accumulations (due to snowfall and blowing snow) are typically greater at RT and FO while increasing their uncertainties. In addition, FO is a problematic HRU in the MC model. Treeline hydrology is very sensitive to blowing snow deposition and interception processes, making it difficult to parameterise. For example, the 2010 SWE is greatly overestimated by the model. Fang *et al*. (2013) investigated the model failure for this year at this HRU. A potential reason for the SWE overestimation is that the blowing snow processes in CRHM do not consider wind direction and in this year synoptic systems may have acted to vary wind direction from the normal, changing the upwind fetch area for FO (Fang *et al.,* 2013).

Among the PSY, UBC and T0 models at the HRU scale, T0 generally predicts more rainfall and less snowfall and runoff than UBC and PSY. The SWE simulations demonstrate the effect of these different PPM biases upon hydrological prediction. T0 estimates less snowfall than UBC, resulting in smaller SWE accumulation than UBC, as shown in Figure 4.3. By contrast PSY, which estimates smaller annual snowfalls than UBC but similar snowfall over the winter season, estimates greater SWE accumulation. This behaviour is due to PSY being dependent upon T_i in contrast to UBC which is dependent on T_a. The difference between T_i and T_a is primarily dependent upon *RH* but the magnitude of the difference increases with warming T_a. Thus winter snowfall identified by PSY will be similar to UBC in contrast to summer snowfall where PSY will predict less snowfall than UBC. PSY identifies slightly more snowfall during the snow accumulation season leading to greater estimates of SWE even though it does not identify greater annual snowfall.

4.5.2 Basin Scale Relationships

The modeled basins vary in terms of climate, topography and area all of which influence the model structure and hydrological processes considered. The uncertainty due to the phase methods can be seen to be largely a function of climate and topography. WC, GB and BL are relatively cold and dry climates while MC is warmer and much wetter. MC, WC and GB have more relief than BL. WC is a large basin (195 km^2) while MC, GB and BL are all relatively small basins. The MC model is the most complex, with 36 HRUs, followed by GB, with 5 HRUs and WC and BL (both having 3 HRUs). The small alpine basins, MC and GB, have the greatest uncertainty in terms of rainfall, snowfall and thereafter snow accumulation processes. The uncertainty of Marmot Creek (1600 m to 2825 m) and Granger Basin (1310 m to 2100 m) can be related to the lapse rates observed, or applied, to the elevation differences between HRUs. With a range of T_a spanning the elevations of a basin, phase methods, both T_a based and psychrometric, have a higher degree of probability than basins with little relief of varying precipitation phase identification across the basin at some elevations in many events. BL, which has little relief, has a much lower uncertainty as T_a is assumed to be uniform over the basin which reduces the uncertainty of rainfall, snowfall and snow processes. All other basins show long periods of phase uncertainty which coincide with large amounts of precipitation, but BL only shows a short period of phase uncertainty in the shoulder months that do not have large depths of precipitation or snowmelt. The duration of phase uncertainty at BL is reduced by the continental climate of the prairies which experiences very cold winter and hot summers with only limited periods of time near the phase thresholds. At a HRU scale, T0 tends to simulate greater values of rain ratio than PSY and UBC although at basin scales PSY rain ratio has greater values in summer and lower values in winter than UBC. PSY results in a sharper distinction in rainfall and snowfall between seasons compared to UBC and is more physically appropriate.

The snow processes at MC, compared to other basins, are generally the most uncertain as a consequence of the direct impact of the increased uncertainty in rain ratio in this basin. The occurrence of most of this basin's precipitation near the transition range means that the SWE simulations are more sensitive to phase methods than other basins. At MC PSY simulated greater peak SWE than did UBC followed by T0. In the GB and WC basins which have colder winters and cooler summers the UBC method simulates less SWE in winter and more in summer than

PSY. UBC assigns summer precipitation as rainfall less frequently than PSY due to the psychrometric nature of PSY which incorporates the lower summer relative humidities. BL shows very little uncertainty, except at the end of the spring melt, in the amount and number of snow free days or duration, due to the climatic extremes. By contrast, the high degree of uncertainty of snowcover duration for WC is attributed to the increased occurrence of snowfall being simulated in summer months due to the cooler weather in northern Canada. The uncertainty of snowcover duration and snow free date at MC is largely due to the occurrence of most precipitation occurring near the transition range, 60% of precipitation occurs between -5 °C and 5 °C at UC, thus any changes in method will have large impacts on the duration of snowcover.

Daily discharge at MC and peak discharge and timing of peak at GB show much greater uncertainty than at other basins. This is believed to be a consequence of climate. MC consistently generates considerably more discharge, thus greater uncertainty, than the other basins which have ephemeral streamflow. By increasing the amount of snowfall and changing some snowfall events to rainfall-runoff events the model can simulate entirely new and separate discharge events in the ephemeral basins. Thus while the daily discharge may vary more at MC, which has more discharge to begin with, the relative differences in discharge for the basins with ephemeral streamflow is much larger. For MC, GB and WC basins, T0 produces the most discharge, and higher and earlier peak flows, followed by PSY and UBC implying that these models are able to produce more discharge with methods that simulate more rainfall. In addition the interaction of phase and precipitation intensity can be important. A high intensity precipitation event identified as snowfall will not have any effects on discharge processes as the snowfall will merely be added to the snowpack, while high intensity precipitation identified as rainfall results in high flow events to be simulated. The spring season in the western cordillera (where MC, GB and WC are located) is typically when high intensity precipitation events occur which coincides with a period of greater phase uncertainty amplifying the uncertainty of discharge from these alpine basins. The prairie basins such as BL are typically ineffective at transforming rainfall into discharge in the summer due to flat topography and soils with large water holding capacities. Therefore methods which identify more snowfall, UBC and PSY, will lead to greater discharge in prairie basins.

4.5.3 Model performance

In the simplest case of the UC model (no interception or blowing snow) the methods that considered mixed phase (UBC) performed better than T0. For the other sites which address interception and blowing snow processes T0 performance is best. The increase in uncertainty due to additional processes masks the improvements in performance caused by using more accurate methods.

CRHM has some difficulty in estimating the hydrograph correctly at MC (Figure 4.11) as it has a tendency to overestimate streamflow response to individual snowmelt or rainfall events and to underestimate the main snowmelt event and can be attributed to problems in the modeling of streamflow routing and soil water processes (Fang *et al.,* 2013). Given that there are problems with timing in routing and groundwater processes, a more appropriate relationship to examine is the comparison of the seasonal observed versus estimated discharge. Most methods tend to produce more discharge than what is observed. In general T0 produces the most discharge followed closely by PSY and finally UBC, and therefore the methods which estimate the most rainfall will lead to greater discharge.

Since CRHM is a physically based model it is useful to diagnose the adequacy of hydrological understanding (Pomeroy *et al.,* 2007). Although empirical methods outperformed PSY this does not mean that empirical methods are necessarily more accurate as they require parameters which are unidentifiable. The range of appropriate rainfall and snowfall T_a threshold parameters is known but as phase-T_a relationships do not have a physical basis it is not possible to accurately determine these parameters for a given case. The simulation of hydrological processes is improved with the PSY phase model which is physically based and has no parameters to set; therefore no uncertainty. The elimination of a previously unknown parameter uncertainty with the PSY method constitutes an improvement in simulation which will lead to correction of previously unknown deficiencies.

4.5.4 Uncertainty Attribution

The uncertainty analysis attributed the differences between basins to the phase partitioning methods. The basins modelled all have different model structures, which may be a source of

some of the uncertainty observed, but these differences are considered negligible for two reasons. First, both small alpine basins (MC and GB) had the highest uncertainty even though the model structures are very different. This shows that the interaction between precipitation phase partitioning methods and basin physiography and climate are consistent regardless of model structure. Second, a test to compare BL to UC (a HRU of MC) with both models using the EBSM snowmelt module reveals the inability of EBSM to model the deep alpine snowcover; EBSM accumulated 2.5 times the snowpack of Snobal; the EBSM snowmelt and albedo models were developed for shallow prairie, not deep alpine, snowcovers. This shows that environments with different manifestations of the same hydrological processes need to be represented with the appropriate models otherwise the uncertainty due to model structure will overwhelm the uncertainty due to different phase partitioning methods. The uncertainty due to differences in model structure, when using the most appropriate process representations, will be secondary to the uncertainty due to the precipitation phase partitioning methods.

4.5.5 Limitations

The approach CRHM uses to assign precipitation phase and amounts are tied to limitations in the analysis of hydrologic uncertainty introduced by differing phase methods. To better assess the impact various methods have on precipitation phase and its uncertainty, CRHM should be run with an independently identified phase dataset. Comparing the independently identified phase method output to other phase methods would give stronger estimates of uncertainty, which is not possible for basins, or sites, where the precipitation phase is not observed. Another limitation exists in the temporal resolution of precipitation data. MC has hourly precipitation data but GB, WC and BL only have daily precipitation data. By using daily precipitation divided across all hours of the day, the mass of water that is entering the basin is conserved but the uncertainty in phase identification is increased. A precipitation event is likely occurring over a period of time shorter than 24 hours, at varying intensities, and thus daily meteorological conditions that identify phase may not correspond to the actual, phase controlling, meteorological conditions in which the precipitation occurred. The time scale dependence of precipitation phase identification demonstrates differences between daily and hourly phase methods of up to 5% of the annual precipitation.

CHAPTER 5. Conclusions

Accurate determination of precipitation phase is important for quantifying snow processes and rainfall-runoff relationships. Falling hydrometeors are subject to turbulent transfer of heat and water vapour with the atmosphere and so T_i, as estimated from the psychrometric mass and energy balance, is a more physically based method of calculating precipitation phase than T_a alone. A psychrometric energy balance calculation of T_i was developed from existing blowing snow sublimation turbulent transfer equations. The relationship between phase and T_a or T_i was examined for several years using a high quality dataset from a Canadian Rockies catchment and found to be time scale dependent, in that there was a smaller mixed-phaseT_i transition range at shorter time intervals; the transition range was 2.9 °C versus 7.6 °C for T_i for 15 minute and daily scale respectively. This suggests that precipitation phase methods, which can adjust for the time step of observations, have increased power at shorter time steps. To take advantage of this temporal scale dependence, the values of T_i estimated by the psychrometric mass and energy balance equation fitted to observations of precipitation phase were used to estimate rainfall fraction at various time steps using a sigmoidal function whose parameters are dependent on the time interval. A detailed examination of precipitation phase dynamics at several elevations in a Canadian Rockies catchment showed that this new method can be a stronger predictor of phase than T_a, with the degree of improvement increasing as the length of the time interval decreases.

Many methods have been used in hydrological modeling to identify precipitation phase and the uncertainty a selection of these methods introduce into hydrological modelling was compared over a variety of basins and scales. The magnitude of the uncertainty associated with T_a models is up to 20% for rain ratio, 1.5 mm for mean daily runoff, 0.4 mm for mean daily discharge and 160 mm of peak SWE. The timing of selected variables showed considerable uncertainty with variations of up to 36 days for the length of snowcover duration, 26 days for snow free date and 10 days for date of peak discharge. The magnitude of the uncertainty among basins was largely a function of climate and topography. The most sensitive basins, due to their having more precipitation occurring in the transition temperature range and their topography influencing T_a lapse rates, were MC and BG, which are small alpine basins. In contrast BL, being flatter and having a more extreme climate showed the least uncertainty in most variables. Generally, those

HRUs which had processes that added mass (FO, which was a blowing snow sink) had greater uncertainty than those that had processes which removed mass (UF, which had snow interception and RT, which was a blowing snow source). Statistical assessment of the performance of the HRU scale SWE simulations did not identify any method to be consistently better than the others; PSY and UBC were very similar and T0 performed better in some situations. Assessment of the simulated seasonal discharges at MC showed that all methods overestimated discharge, with UBC doing the best. The uncertainty introduced with setting unidentifiable parameters for empirical methods is reduced with PSY, which has no parameters to set. The relationship between empirical and physically based methods is temporally variable resulting in complex relationships between empirically and physically based hydrologic simulations. Errors in the identification of precipitation phase constitute a significant source of potential error in hydrological modeling and this uncertainty has been underappreciated in previous research.

Although PSY was shown to work well at MC the spatial transferability of the model needs further study. Testing of PSY against precipitation phase observations in areas that experience differing synoptic and climatic conditions is needed. Potential sites are limited to locations where high quality hydrometeorological observations exist, especially observations of precipitation phase. By extending application of the PSY to other regions an understanding of its spatial transferability will be gained. The semi-physical basis of the method and its testing in MC suggest that it will be a more reliable method in other locations but this needs to be confirmed.

A semi-physical precipitation phase model, rather than empirical T_a methods, provides more accurate and less uncertain estimates of precipitation phase. The dynamic nature of meteorology within precipitation events affects the on accuracy of methods; thus phase should be estimated on hourly time steps, which corresponds to the recording interval of most modern meteorological stations. The uncertainty introduced by phase methods is observed to propagate and increase in magnitude through the model with each transformation of mass, from snowfall to snowpack to snowmelt discharge. The quantification of the phase uncertainty clearly shows that the hydrological modeling community needs be aware of the effects, uncertainty and errors associated with using T_a phase methods. The proposed semi-physical psychrometric method provides a more accurate alternative that can be easily implemented in hydrological models.

REFERENCES

AESRD. 2013. Alberta Environment and Sustainable Resource Development June 19-22 2013 Precipitation Map. Accessible at: http://www.environment.alberta.ca/forecasting/data/precipmaps/event.pdf [August 23, 2013]

Annandale JG, Jovanovic NZ, Benadé N, Allen RG. 2004. Software for missing data analysis of Penman-Monteith reference evapotranspiration. *Irrig. Sci* 21: 57–67.

Auer AH. 1974. The Rain versus Snow Threshold Temperatures. *Weatherwise* 27: 67.

Ayers HD. 1959. Influence of soil profile and vegetation characteristics on net rainfall supply to runoff. In *Proceedings of Hydrology Symposium No. 1: Spillway Design Floods*. National Research Council Canada; Ottawa. 198–205

Beck MB. 1987. Uncertainty in water quality models. *Wat. Res. Res.* 23: 1393.

Bicknell BR, Imhoff JC, Kittle JL, Donigian AS, Johanson RC. 1997. *Hydrological Simulation Program-Fortran: User's Manual for Version 11.* EPA/600/R-97/080. U.S. Environmental Protection Agency, National Exposure Research Laboratory, Athens, Ga; 755.

Brooks RH, Corey AT. 1964. Hydraulic properties of porous media. Hydrology paper No. 3, Colorado St. Univ., Fort Collins.

Buck A. 1981. New Equations for Computing Vapor Pressure and Enhancement Factor. *Journal of Applied Meteorology* 20: 1527-1532.

Clark CO. 1945. Storage and the unit hydrograph. *Proceedings of American Society of Civil Engineering* 69: 1419–1447.

Chow VT.1964. *Handbook of Applied Hydrology*, McGraw-Hill, Inc.; New York.

Dingman S. 2002. *Physical Hydrology* (2nd ed.). Prentice Hall; Upper Saddle River, New Jersey; 646.

Dornes PF, Pomeroy JW, Pietroniro A, Carey SK, Quinton WL. 2008. Influence of landscape aggregation in modelling snow-cover ablation and snowmelt runoff in a subarctic mountainous environment. *Hydrological Sciences Journal* 53: 725–740.

Ellis CR, Pomeroy JW, Brown T, MacDonald J. 2010. Simulation of snow accumulation and melt in needle leaf forest environments. *Hydrology and Earth System Sciences* 14: 925–940.

Fang X, Pomeroy JW, Westbrook CJ, Guo X, Minke AG, Brown T. 2010. Prediction of snowmelt derived streamflow in a wetland dominated prairie basin. *Hydrology and Earth System Sciences* 14: 991-1006.

Fang X, Pomeroy JW, Ellis CR, MacDonald MK, DeBeer CM, Brown T. 2013. Multi-variable evaluation of hydrological model predictions for a headwater basin in the Canadian Rocky Mountains. *Hydrol. Earth Syst. Sci. Discuss*. 17: 1635-1659.

Fassnacht SR, Kouwen N, Soulis ED. 2001. Surface Temperature Adjustment to Improve Weather Radar Representation of Multi-Temporal Winter Precipitation Accumulation. *Journal of Hydrology* 253: 148–168.

Fassnacht SR, Soulis ED. 2002. Implications during transitional periods of improvements to the snow processes in the land surface scheme - hydrological model WATCLASS. *Atmosphere-Ocean*: 40, 389-403.

Feiccabrino J, Lundberg A. 2008. Precipitation Phase Discrimination in Sweden. In *65th Eastern Snow Conference.* Fairlee (Lake Morey), Vermont, USA; 239–254.

Fuchs D. 2006. Temperature Analyses of Days with Precipitation in Alpine Regions. M.Sc. Thesis. Institute of Meteorology and Geophysics. University of Innsbruck: Innsbruck, Austria; 154.

Garnier BJ, Ohmura A. 1970. The evaluation of surface variations in solar radiation income. *Solar Energy* 13: 21–34.

Gatley D. 2004. Psychrometric Chart Celebrates 100th Anniversary. *ASHRAE Journal* Nov.: 16-20.

Gjertsen U, Odegaard V. 2005. The Water Phase of Precipitation—a Comparison between Observed, Estimated and Predicted Values. *Atmospheric Research* 77: 218–231.

Goodison, BE. 1978. Accuracy of Canadian Snow Gage Measurements. *Journal of Applied Meteorology* 17: 1542-1548.

Granger RJ, Gray DM. 1989. Evaporation from natural non-saturated surfaces. *Journal of Hydrology* 111: 21–29.

Granger RJ, Gray DM. 1990. A net radiation model for calculating daily snowmelt in open environments. *Nordic Hydrology* 21: 217–234.

Granger RJ, Pomeroy JW. 1997. Sustainability of the western Canadian boreal forest under changing hydrological conditions—2-summer energy and water use. In *Sustainability of Water Resources under Increasing Uncertainty*, Rosjberg D, Boutayeb N, Gustard A, Kundzewicz Z, Rasmussen P (eds). IAHS Publ No. 240. IAHS Press: Wallingford; 243–250.

Gray DM. 1970. *Handbook on the Principles of Hydrology*. Water Information Center: New York, USA; 691.

Gray DM, Granger RJ. 1986. In situ measurements of moisture and salt movement in freezing soils. *Canadian Journal of Earth Sciences* 23: 696–704.

Gray DM, Landine PG. 1987. Albedo model for shallow prairie snowcovers. *Canadian Journal of Earth Sciences* 24: 1760–1768.

Gray DM, Landine PG. 1988. An energy-budget snowmelt model for the Canadian prairies. *Canadian Journal of Earth Sciences* 25: 1292–1303.

Gray DM, Landine PG, Granger RJ. 1985. Simulating infiltration into frozen Prairie soils in stream flow models. *Canadian Journal of Earth Science* 22: 464–474.

Gray DM, Prowse TD. 1992. Snow and Floating Ice. In *The Handbook of Hydrology*, Maidment DR (ed). McGraw-Hill Publishing Co.: New York, New York, USA; 631–653.

Gray DM, Toth B, Pomeroy JW, Zhao L, Granger RJ. 2001. Estimating areal snowmelt infiltration into frozen soils. *Hydrological Processes* 15: 3095-3111.

Harder P, Pomeroy JW, Westbrook CJ. 2013. Climate Change and Forest Management Impacts on the Hydrometeorology of a Canadian Rockies Headwaters Basin. Poster presentation at the CGU Annual Meeting, Saskatoon SK, May 26-30.

Janowicz JR. 1999. Wolf Creek Research Basin – an overview. In *Wolf Creek Research Basin: Hydrology, Ecology, Environment*, Pomeroy JW, Granger R (eds). Environment Canada: Saskatoon; 121-130.

Kienzle SW. 2008. A New Temperature Based Method to Separate Rain and Snow. *Hydrological Processes* 5085: 5067– 5085.

Kinzer G, Gunn R. 1951. The Evaporation, Temperature and Thermal Relaxation-Time of Freely Falling Waterdrops. *Journal of Meteorology* 8: 71-83.

Lamb H, Durocher Y. 2004. Weight Gauge Algorithms. In *61sy Eastern Snow Conference.* Portland, Maine, USA; 27-53.

Leavesley GH, Lichty RW, Troutman BM, Saindon LG. 1983. *Precipitation-runoff modelling system: User's Manual*. Report 83-4238. US Geological Survey Water Resources Investigations; 207.

Lee LW. 1975. Sublimation of Snow in Turbulent Atmosphere. Ph.D. Thesis, University of Wyoming, Laramie, 162.

Li L, Pomeroy JW. 1997. Estimates of Threshold Wind Speeds for Snow Transport Using Meteorological Data. *Journal of Applied Meteorology* 36: 205–213.

Livingstone A. 2013. Alberta Floods: Assessing the human, environmental and economic impact. *The Star* [Toronto] 24 June.

Loth B, Graf H, Oberhuber J. 1993. Snow Cover Model for Global Climate Simulations. *Journal of Geophysical Research* 98: 10451-10464.

Lynch-Stieglitz M. 1994. The development and validation of a simple snow model for the GISS GCM. *J. Clim*. 7: 1842–1855.

MacDonald JP, Pomeroy JW. 2007. Gauge Undercatch of Two Common Snowfall Gauges in a Prairie Environment. In *Proceedings of the 64th Eastern Snow Conference,* St. John's, Newfoundland, Canada*:* 119–126.

MacDonald MK, Pomeroy JW, Pietroniro A. 2009. Parameterising redistribution and sublimation of blowing snow for hydrological models: tests in a mountainous subarctic catchment. *Hydrological Processes;* OI:10.1002/hyp.7356.

Marks D, Domingo J, Susong D, Link T, Garen D. 1999. A spatially distributed energy balance snowmelt model for application in mountain basins. Hydrological Processes 13: 1935-1959.

Marks D, Kimball J, Tingey D, Link T. 1998. The sensitivity of snowmelt processes to climate conditions and forest cover during rain-on-snow: a case study of the 1996 Pacific Northwest Flood. *Hydrological Processes* 12: 1569–1587.

Marks D, Winstral A, Reba M, Pomeroy J, Kumar M. 2013. An Evaluation of Methods for Determining During-Storm Precipitation Phase and the Rain/Snow Transition Elevation at the Surface in a Mountain Basin. *Advances in Water Resources* http://dx.doi.org/10.1016/j. advwatres.2012.11.012.

McIntyre N, Wheater H, Lees M. 2002. Estimation and propagation of parametric uncertainty in environmental models. *Journal of Hydroinformatics* 4.3: 177-198.

Melching C. 1995. Reliability estimation. in *Computer Models of Watershed Hydrology*, Singh VP (ed.). Water Resource Publications, New York: 69–118.

Milly PCD, Betancourt J, Falkenmark M, Hirsch RM, Kundezewicz ZW, Lettenmaier DP, Stouffer RJ. 2008. Stationarity Is Dead: Whither Water Management? *Science* 319: 573-574.

Minder JR, Durran DR, Roe GH. 2011. Mesoscale Controls on the Mountainside Snow Line. *Journal of the Atmospheric Sciences* 68: 2107-2127.

Monteith J, Unsworth M. 2008. Principles of Environmental Physics(3rd ed.). Elsevier: Amsterdam; 440.

Mote PW, Hamlet AF, Clark P, Lettenmaier DP. 2005. Declining Mountain Snowpack in Western North America. *Bulletin of the American Meteorological Society* 86: 39–49.

Nayak A, Chandler DG, Marks D, McNamara JP, Seyfried M. 2008. Correction of electronic record for weighing bucket precipitation gauge measurements. *Water Resources Research* 44, W00D11, doi:10.1029/2008WR006875.

Olafsson H, Haraldsdottir SH. 2003. Diurnal, Seasonal, and Geographical Variability of Air Temperature Limits of Snow and Rain. In *Proceedings of ICAM/MAP 2003.* Brig, Switzerland: 473-476.

Olsen A. 2003. Snow or rain?: A Matter of Wet-Bulb Temperature. M.Sc. Thesis. Institute for Earth Sciences, Uppsala University: Uppsala, Sweden; 32.

Pietroniro A, Fortin V, Kouwen N, Neal C, Turcotte R, Davison B, Verseghy D, Soulis ED, Caldwell R, Evora N, Pellerin P. 2007. Development of the MESH modelling system for hydrological ensemble forecasting of the Laurentian Great Lakes at the regional scale. *Hydrology and Earth System Science* 11: 1279–1294.

Pipes A, Quick M. 1977. *UBC Watershed Model Users Guide*. Department of Civil Engineering, University of British Columbia.

Pomeroy JW, Fang X, Ellis CR. 2012. Sensitivity of snowmelt hydrology in Marmot Creek, Alberta, to forest cover disturbance. *Hydrological Processes* 26: 1891–1904. doi: 10.1002/hyp.9248.

Pomeroy JW, Granger RJ. 1999. *Wolf Creek Research Basin: Hydrology, Ecology, Environment*. Environment Canada, Saskatoon, Canada: 160.

Pomeroy JW, Gray DM. 1995. *Snow Accumulation, Relocation and Management*. National Hydrology Research Institute Science Report No. 7. Environment Canada: Saskatoon; 144.

Pomeroy JW, Gray DM, Brown T, Hedstrom NR, Quinton W, Granger RJ, Carey S. 2007. The cold regions hydrological model: a platform for basing process representation and model structure on physical evidence. *Hydrological Processes* 21: 2650–2667. DOI: 10.1002/hyp.6787.

Pomeroy JW, Gray DM, Landine PG. 1993. The Prairie Blowing Snow Model: Characteristics, Validation, Operation. *Journal of Hydrology* 144: 165–192.

Pomeroy JW, Li L. 2000. Prairie and Arctic areal snow cover mass balance using a blowing snow model. *Journal of Geophysical Research* 105(D21): 26619–26634.

Pomeroy JW, Parviainen J, Hedstrom N, Gray D M. 1998. Coupled modelling of forest snow interception and sublimation, *Hydrol. Process.* 12: 2317–2337.

Pomeroy JW, Semenova OM, Vinogradov YB, Chad E, Vinogradova, TA, Macdonald M, Fisher EE, Dornes P, Lebedeva L, Brown T. 2010. Wolf Creek Cold Regions Model Set-up, Parameterisation and Modelling Summary. Centre for Hydrology Report No. 8. University of Saskatchewan; Saskatoon, Saskatchewan: 107.

Priestley CHB, Taylor RJ. 1972. On the assessment of surface heat flux and evaporation using large-scale parameters. *Mon. Weather Rev.* 100: 81-92.

Rogers RR, Yau MK. 1989. *A Short Course in Cloud Physics* (3rd ed.) Butterworth–Heinemann: Burlington, MA; 304.

Saelthun NR, 1996. *The "Nordic" HBV-Model. Description and Documentation of the Model Version Developed for the Project Climate Change and Energy Production*. NVE, 7: Oslo.

Schmidt RA. 1972. *Sublimation of Wind-Transported Snow - A Model*. Research Paper RM-90, U.S. Department of Agriculture Forest Service, Rocky Mountain Forest and Range Experiment Station: Fort Collins, Colorado, USA.

Sicart JE, Pomeroy JW, Essery RLH, Bewley D. 2006. Incoming longwave radiation to melting snow: observations, sensitivity and estimation in northern environments. *Hydrological Processes 20*:3697-3708.

Shook KR, Pomeroy JW. 2011. Synthesis of incoming shortwave radiation for hydrological simulation. *Hydrology Research* 42: 433.

Steinacker R. 1983. Diagnose und Prognose der Schneefallgrenze. *Wetter & Leben* 35: 81–90.

Stewart RE. 1992. Precipitation Types in the Transition Region of Winter Storms. *Bulletin American Meteorological Society* 73: 287–296.

Storr D. 1967. Precipitation Variations in a Small Forested Watershed. In *Proceedings of the Annual Western Snow Conference*, Boise, Idaho: 11– 17.

Sugaya H. 1991. Distinguishing between Rain and Snow in Cold Season (3), Prediction with the Wet-Bulb Temperature. In *Proceedings of 1991 Annual Meeting of the Japanese Society of Snow and Ice*; 48.

Swanson RH, Golding DL, Rothwell RL, Bernier PY. 1986. *Hydrologic effects of clear-cutting at Marmot Creek and Streeter watersheds, Alberta.* Northern Forestry Centre Information Report NOR-X-278, Canadian Forestry Service: Edmonton, Alberta; 33.

Tardif R, Rasmussen RM, 2010, Evaporation of Nonequilibrium Raindrops as a Fog Formation Mechanism. *Journal of the Atmospheric Sciences* 67: 345–364.

Thériault JM, Rasmussen R, Ikeda K, Landolt S. 2012. Dependence of Snow Gauge Collection Efficiency on Snowflake Characteristics. *Journal of Applied Meteorology and Climatology* 51:745-762.

Thériault JM, Stewart RE. 2010. A Parameterization of the Microphysical Processes Forming Many Types of Winter Precipitation. *Journal of the Atmospheric Sciences* 67: 1492–1508.

Thorpe AD, Mason BJ. 1966. The Evaporation of Ice Spheres and Ice Crystals. *British Journal of Applied Physics* 17: 541-548.

Tung, Y. K. 1996 Uncertainty and reliability analysis. in *Water Resources Handbook*, Mays L W (ed.). McGraw-Hill, New York: 7.1–7.65.

US Army Corps of Engineers. 1956. *Snow Hydrology: Summary Report of the Snow Investigations*. North Pacific Division: Portland Oregon, USA; 437.

Verseghy, DL. 1991 CLASS-A Canadian land surface scheme for GCMs, I. soil model, *Int. J. Climatol.* 11: 111–133.

Wen L, Nagabhatla N, Lv S, Wang S. 2013, Impact of rain snow threshold (RST) temperature on snow depth simulation in land surface model and regional climate model. *Advances in Atmospheric Sciences* (accepted)

Yamazaki T. 2001. A One-dimensional Land Surface Model Adaptable to Intensely Cold Regions and its Applications in Eastern Siberia. *Journal of the Meteorological Society of Japan* 79: 1107–1118.

Zehe E, Becker R, Bardossy A, Plate E. 2005. Uncertainty of simulated catchment runoff response in the presence of threshold processes: Role of initial soil moisture and precipitation. *Journal of Hydrology* 315: 183–202.

Zhao L, Gray DM. 1999. Estimating snowmelt infiltration into frozen soils. *Hydrological Processes* 13: 1827–1842.

APPENDIX A: Hourly Psychrometric Phase Parameterisation: CRHM Macro

```
Rain_Snow_Icebulb PH 03/21/2013
declgetvar,*, hru_t, (°C)
declgetvar,*, hru_rh, (%),
declgetvar,*, hru_p, (mm/int)
declputvar, *, hru_rain,(mm/int)
declputvar, *, hru_snow,(mm/int)
declputvar, *, cumhru_rain,(mm)
declputvar, *, cumhru_snow,(mm)
declputvar, *, hru_newsnow,(), int
declvar,hru_icebulb, NHRU, "Estimates ice bulb temperature", (°C)
declvar,ratio, NHRU, "rain/snow ratio", (%),Int
decllocal,D, NHRU, "Diffusivity", ()
decllocal,L, NHRU, "Latent Heat", (J/kg)
decllocal,lamda, NHRU, "thermal conductivity", ()
decllocal,pta, NHRU, "atmospheric specific humidity", ()
decllocal,Ti1, NHRU, "Initial guess of Ti", ()
decllocal,T1, NHRU, "Newton-Raphston iteration slope1", ()
decllocal,T2, NHRU, "Newton-Raphston iteration slope2", ()
decllocal,Ti2, NHRU, "Ti resulting from Ti1", ()
decllocal,crit, NHRU, "absolute value of crit1 threshold", ()
decllocal,crit1, NHRU, "difference between Ti1 and Ti2", ()
decllocal,Tk, NHRU, "Temperature in Kelvin", ()
decllocal,a, NHRU, "Newton-Raphston term for Ti1", ()
decllocal,b, NHRU, "Newton-Raphston term for T1", ()
decllocal,c, NHRU, "Newton-Raphston term for T2", ()
command
Tk[hh] = hru_t[hh]+273.15
D[hh] = 0.0000206*(Tk[hh]/273.15)^1.75
lamda[hh] = 0.000063*Tk[hh]+0.00673
pta[hh] =
18.01528*((hru_rh[hh]/100)*0.611*exp((17.3*hru_t[hh])/(237.3+hru_t[hh])))/(0.00831441*(hru
_t[hh]+273.15))/1000
if(hru_t[hh] > 0.0)
     L[hh] = 1000*(2501-(2.361*hru_t[hh]))
   else
     L[hh] = 1000*(2834.1-0.29*hru_t[hh]-0.004*hru_t[hh]^2)
endif
Ti1[hh] = 250
```

```
crit[hh] = 9999
while(crit[hh] > 0.0001)
T1[hh] = Ti1[hh]+0.001*Ti1[hh]
T2[hh] = Ti1[hh]-0.001*Ti1[hh]
a[hh]=(-Ti1[hh]+Tk[hh]+(L[hh]*D[hh]/lamda[hh])*(pta[hh]-
(18.01528*(0.611*exp((17.3*(Ti1[hh]-273.15))/(237.3+(Ti1[hh]-
273.15))))/(0.00831441*Ti1[hh])/1000)))
b[hh]=(-T1[hh]+Tk[hh]+(L[hh]*D[hh]/lamda[hh])*(pta[hh]-
(18.01528*(0.611*exp((17.3*(T1[hh]-273.15))/(237.3+(T1[hh]-
273.15))))/(0.00831441*T1[hh])/1000)))
c[hh]=(-T2[hh]+Tk[hh]+(L[hh]*D[hh]/lamda[hh])*(pta[hh]-
(18.01528*(0.611*exp((17.3*(T2[hh]-273.15))/(237.3+(T2[hh]-
273.15))))/(0.00831441*T2[hh])/1000)))
Ti2[hh]= Ti1[hh]-(a[hh]/((b[hh]-c[hh])/(0.002*Ti1[hh])))
crit1[hh] = Ti1[hh]-Ti2[hh]
if(crit1[hh] < 0)
crit[hh]= crit1[hh]*-1
else
crit[hh]= crit1[hh]
endif
Ti1[hh] = Ti2[hh]
endwhile
hru_icebulb[hh] = Ti1[hh]-273.15
if(hru_icebulb[hh]<-10)//Eoverflow if ratio calculated with icebulb < -39C
ratio[hh]=0
else
ratio[hh]=(1/(1+2.50286*0.125006^hru_icebulb[hh]))*100
endif
hru_snow[hh] = 0.0
hru_rain[hh] = 0.0
if(hru_p[hh] > 0.0) //rain or snow determined by ice bulb ratio
hru_rain[hh] = hru_p[hh]*(ratio[hh]/100)
hru_snow[hh] = hru_p[hh]*((100-ratio[hh])/100)
if(hru_snow[hh] > 0.0)
hru_newsnow[hh] = 1
else
hru_newsnow[hh] = 0
endif
endif
end
```

APPENDIX B: Hydrometeor Temperature Solution: R Code

```
################################################
#Hydrometeor Temperature (Ti) Iterative Solution
#R Code
#October 17, 2013
#Phillip Harder
################################################

#Input
Ta<--10 #Air Temperature [C]
RH<-75 #Relative Humidity wrt to water [%]

#Constants
mw<- 18.01528 #Molar mass of water [gmol-1]
Ru<-0.00831441 #Universal gas constant [m3kPag-1mol-1K-1]

#Corrections with respect to Ta
#Latent Heat [J kg-1]
if(Ta > 0){
L<-1000*(2501-(2.361*Ta))
} else {
 L<-1000*(2834.1-0.29*Ta[which(Ta<0)]-0.004*Ta[which(Ta<0)]^2)
}
#Buck (1981) correction for saturation wrt to ice when Ta < 0 C
if(Ta<0){
 ew<-(RH/100)*0.61121*exp((17.502*Ta)/(240.97 + Ta))# actual vapour pressure wrt to water
[kPa]
 eisat<-0.61115*exp((22.452*Ta)/(272.55+Ta))# saturated vapour pressure wrt to ice [kPa]
 RH<-(ew/eisat)*100
}

#Functions
#water vapour density (ASHRAE,1993)[gm-3]
phivfun<-function(mw,RH,Ta,Ru){
 phiv<-mw*(RH/100*0.611*exp((17.3*Ta)/(237.3+Ta)))/(Ru*(Ta+273.15))/1000
}
#saturated water vapour density (ASHRAE,1993)[gm-3]
phivtfun<-function(mw,Ta,Ru){
 phivt<-mw*(0.611*exp((17.3*Ta)/(237.3+Ta)))/(Ru*(Ta+273.15))/1000
}
```

```
#Diffusivity of water vapour in air [m2 s-1]
Dvfun<-function(Ta){
 Dv<-2.06*10^-5*((Ta+273.15)/273.15)^1.75
}
#Thermal conductivity of air [J m-1 s-1 K-1]
Kafun<-function(Ta){
 Ka<-0.000063*(Ta+273.15)+0.00673
}
#Newton-Raphston Iteration Functions
ffun<-function(Ta,Ti1){
 ff<--Ti1+Ta-(L*Dvfun(Ta)/Kafun(Ta))*(phivtfun(mw,Ti1,Ru)-phivfun(mw,RH,Ta,Ru))
}
fpfun<-function(Ta,Ti1){
 T1<-Ti1+0.001*Ti1
 T2<-Ti1-0.001*Ti1
 fp<-(ffun(Ta,T1)-ffun(Ta,T2))/(0.002*Ti1)
}
Tifun<-function(Ti1){
 Ti2<-Ti1-ffun(Ta,Ti1)/fpfun(Ta,Ti1)
}

#Ti Iterative Solution
Ti1<-Ta-5.0001 #Initial guess of Ti
crit<-99999 #Initial critical value for while loop
while(crit>0.000001){
 Ti2<-Tifun(Ti1)
 crit<-abs(Ti1-Ti2)
 Ti1<-Ti2
}
Ti<-Ti1
Ti #Hydrometeor Temperature [C]
```